

SLAC-PUB-4601
April 1988
(T/E)

Theory of e^+e^- Collisions at Very High Energy

MICHAEL E. PESKIN*

*Stanford Linear Accelerator Center
Stanford University, Stanford, California 94309*

Lectures presented at the SLAC Summer Institute on Particle Physics
Stanford, California, August 10 – August 21, 1987

* Work supported by the Department of Energy, contract DE-AC03-76SF00515.

1. Introduction

The past fifteen years of high-energy physics have seen the successful elucidation of the strong, weak, and electromagnetic interactions and the explanation of all of these forces in terms of the gauge theories of the standard model. We are now beginning the last stage of this chapter in physics, the era of direct experimentation on the weak vector bosons. Experiments at the CERN $p\bar{p}$ collider have isolated the W and Z bosons and confirmed the standard model expectations for their masses. By the end of the decade, the new colliders SLC and LEP will have carried out precision measurements of the properties of the Z boson, and we have good reason to hope that this will complete the experimental underpinning of the structure of the weak interactions.

Of course, the fact that we have answered some important questions about the working of Nature does not mean that we have exhausted our questions. Far from it! Every advance in fundamental physics brings with it new puzzles. And every advance sets deeper in relief those very mysterious issues, such as the origin of the mass of electron, which have puzzled generations of physicists and still seem out of reach of our understanding. With every major advance, though, we have a chance to review our strategy for probing deeper into the laws of physics, and, indeed, we are obliged to rethink which new questions are the most pressing, and which avenues for further research have the most promise.

In these lectures, I will review the array of new phenomena which might be discovered in electron-positron reactions conducted at energies well above the Z^0 . Before beginning a discussion of what new phenomena we might find, or how we might uncover them, I would like to address the question of why such a program of research is important. I will argue the question of what we should be looking for, and what discoveries will be the most illuminating, as we search for the next layer of fundamental physics. With this background, we can then discuss in some considerable detail the contributions that the study of electron-positron collisions at high energy can make in this search.

1.1. OUR PRESSING QUESTION

Toward what question, then, should we orient ourselves in the next era of high-energy physics? Many authors have given arguments toward a particular conclusion, and of these the most cogent is the case made by Lev Okun in his talk at the 1981 Lepton-Photon conference.^[1] Okun represented our understanding of the fundamental interactions in terms of complementarity—yin and yang—according to the scheme of Fig. 1. On the one side, we have the couplings of

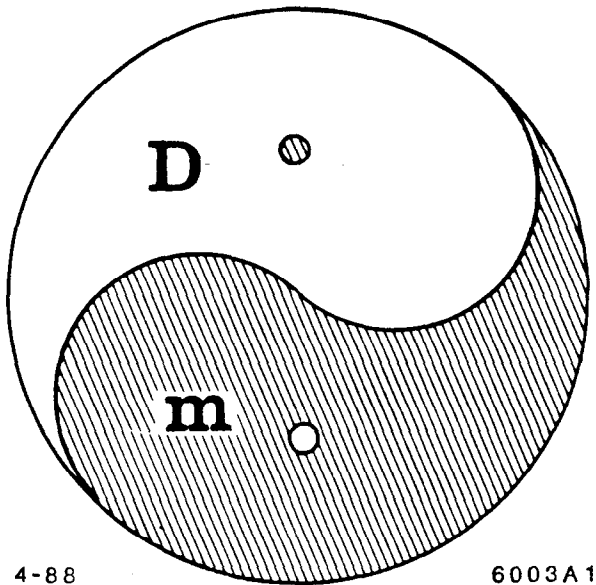


Figure 1. Schematic presentation of the standard model, after L. B. Okun, Ref. 1.

matter to gauge vector bosons, characterized by the gauge-covariant derivative

$$D_\mu = (\partial_\mu - igA_\mu \cdot T - ig'B_\mu Y) . \quad (1.1)$$

This equation represents everything that we understand about the weak interactions. The beauty of the description of the weak interactions in terms of unified gauge theories comes precisely in the fact that the form of the interaction is com-

pletely determined by the local symmetry group $SU(2) \times U(1)$. The complementary property is the generation of masses for fermions and vector bosons. Here the formula is completely unsatisfactory:

$$m = \{g, \lambda, \text{etc.}\} \cdot \langle \Phi \rangle , \quad (1.2)$$

where g and λ are some coupling constants and $\langle \Phi \rangle$ is a parameter carrying mass dimensions, usually called the 'Higgs vacuum expectation value'. From a physical point of view, the origin of this mass parameter, and hence the origin of all masses in the standard model, is a complete mystery.

Actually, the standard model itself gives us some information on the nature of $\langle \Phi \rangle$. Because the weak vector bosons are gauge bosons, they can acquire mass only if the gauge symmetry of the standard model is spontaneously broken. In that case, the vector boson masses are generated by the Higgs mechanism. The mass of the W boson can be written

$$m_W = \frac{1}{2} g \langle \Phi \rangle , \quad (1.3)$$

where g is the gauge coupling constant appearing in (1.1) and $\langle \Phi \rangle$ characterizes the strength of $SU(2) \times U(1)$ breaking. The simplest mechanical model of this effect postulates one $SU(2)$ doublet of scalar fields

$$\varphi = \begin{pmatrix} \varphi^+ \\ \varphi^0 \end{pmatrix} \quad (1.4)$$

with a potential energy function minimized at the value

$$\langle \varphi \rangle = \begin{pmatrix} 0 \\ \frac{1}{\sqrt{2}} \langle \Phi \rangle \end{pmatrix} . \quad (1.5)$$

Even within so simple a model, however, many physical properties are left unexplained. The masses of fermions and of the physical neutral scalar are given by

formulae

$$m_f = \frac{\lambda_f}{\sqrt{2}} \langle \Phi \rangle, \quad m_H = \sqrt{\lambda} \langle \Phi \rangle, \quad (1.6)$$

where the dimensionless coupling constants λ_f , λ are not predicted by the theory and may be adjusted by hand.

In general, this line of analysis gives us very little information about the origin of masses. We learn from (1.3) that $\langle \Phi \rangle$ has the value

$$\langle \Phi \rangle = 250 \text{ GeV}. \quad (1.7)$$

From the striking experimental phenomenon that

$$\rho = m_W^2 / (m_Z^2 \cos^2 \theta_w) = 1 \quad (1.8)$$

to an accuracy better than 1%, we learn that the dynamics which gives rise to the W and Z masses should have its own $SU(2)$ global symmetry.^[2,3] But here our concrete knowledge ends. The one other conclusion on which we can build is that whatever physics gives rise to $\langle \Phi \rangle$ acts on the standard model gauge theory from outside. Thus, $\langle \Phi \rangle$ signals the presence of a new sector of forces and interactions—the Higgs sector. This sector of Nature adds on to the known sectors of matter and gauge forces. It is waiting to be discovered.

Even if we have no certain knowledge of the nature of this Higgs sector, we can explore the range of possibilities given by theoretical models. These generally fall into one of four classes. In the first two, the Higgs mechanism is generated by a set of scalar fields with a potential energy function given *a priori*. In the *minimal* scenario, there exists one doublet of scalar fields, as described in the paragraph above. After spontaneous symmetry breaking and vector boson mass generation, the Higgs sector contains one physical neutral scalar H^0 . The couplings of this particle to matter fermions and to itself determine the masses of those particles, according to (1.6). Unfortunately, the model does not predict the values of these

coupling constants, except to place rather weak bounds on their values. In a *non-minimal* scenario, one would add further doublets of scalars. Each additional doublet adds four more physical scalars (H^+ , H^- , H_1^0 , H_2^0) and also increases the number of undetermined free parameters. The simplest extensions of the standard model, then, have a maddening lack of predictive power.

On the other hand, models which actually explain the breaking of $SU(2) \times U(1)$ tend to be quite complex. These models again are of two types. In the *weak-coupling* scenario, the field whose condensation drives the symmetry breaking is an elementary scalar particle, linked to other particles by interactions which are constrained by some new form of symmetry. The most successful models of this type are supersymmetric theories, in which the Higgs scalars acquire a symmetry-breaking potential energy through their interaction with other forms of super-matter. The mass scale $\langle\Phi\rangle$ of $SU(2) \times U(1)$ breaking is, in general, set by the scale of supersymmetry breaking. In the *strong-coupling* scenario, the Higgs scalar is a composite state, and its condensation is driven by a new set of strong interactions. Technicolor models, in which $SU(2) \times U(1)$ is broken by a fermion pair condensate, belong to this class. In models of this type, the scale $\langle\Phi\rangle$ is determined by the new strong interactions, which must then appear at or even below 1 TeV.

I find it compelling that the phenomenon of $SU(2) \times U(1)$ breaking is a phenomenon of dynamical origin and not simply a feature to be parametrized. Whatever the dynamical mechanism might be, this idea has important consequences for future particle experiments:

1. There exists a new sector of particles, communicating by new forces, beyond the particles of the standard model.
2. The mass scale $\langle\Phi\rangle = 250$ GeV sets the scale of masses and symmetry breaking effects within this new sector.

This sector might contain only a few particles, but it is more likely to be very rich. In particular, the symmetries which must be broken to generate $\langle\Phi\rangle$ can easily protect a variety of other new particles from acquiring masses much larger than

$\langle\Phi\rangle$. Table 1 lists a number of possible states which might gain mass just at the weak interaction scale, depending on what precisely is the fundamental symmetry of the Higgs sector.

Table 1: Possible new particles in the TeV region, and the symmetries which would constrain their masses

<u>Particles:</u>	<u>Protected by:</u>
new quarks and leptons	$SU(2) \times U(1)$
new Z^0	$SU(1)'$
squarks, sleptons	supersymmetry
exotic fermions	$SU(2) \times U(1), U(1)'$
techni-pions, H^\pm	chiral $SU(N)$ of new strong interactions

This conclusion is often expressed in a slightly different language: If one assumes that the fundamental interactions have a grand unification at energies of 10^{15} – 10^{19} GeV, one needs to explain why the weak interaction scale is so much lower than this more basic scale of masses. In any natural explanation, the weak-interaction condensation is forbidden by some symmetry which is broken only below 1 TeV. That symmetry, again, can protect many other states of the grand unified theory from acquiring large masses; these states should then appear in experiments at the weak scale.

Whichever way one expresses the argument, the conclusion is the same: Accompanying the weak-interaction symmetry breaking, there should exist a class of new particles—the ‘TeV multiplet’. These particles should be light enough to be detected in the coming generations of collider experiments. The exact nature of these particles reflects the underlying symmetry of the Higgs sector and points to the mechanism of $SU(2) \times U(1)$ breaking. That is, the properties of these particles identify directly the next extension of the fundamental interactions. I consider it the most pressing problem in high-energy experimentation to discover these particles and determine their quantum numbers.

1.2. OVERVIEW OF THESE LECTURES

In these lectures, I will consider the reactions in high-energy electron-positron colliders which will enable us to discover and characterize these new states. My analysis builds on earlier work along these lines reported in Refs. 4-8, and on the work of an ongoing study at SLAC. The analogous question for pp colliders has also been studied in considerable detail; the basic results have been reviewed in the lectures of Chris Quigg at this school^[9] and the exhaustive review article of Eichten, Hinchliffe, Lane, and Quigg.^[10] I should begin, then, by reviewing the relative advantages and disadvantages of experimentation by e^+e^- reactions.

There are three important advantages in probing new physics through e^+e^- reactions:

1. *The elementary processes are s -channel, nonstrong interactions.* Thus the basic event topologies, both for signal and backgrounds, are very simple. Peripheral reactions, such as the two-photon process, generally have small cross sections.
2. *Familiar and exotic particles are produced democratically.* Thus signal-to-background ratios are generally large, even before restrictive cuts are imposed.
3. *Polarization effects are large and measureable.* At least in linear e^+e^- colliders, it is straightforward to longitudinally polarize the electron beam. This gives an additional, quite interesting method for probing new physics.

These three properties contribute to an experimental environment which is exceptionally clean and which allows unambiguous identification of novel effects. The degree of cleanliness which should be achievable in TeV-energy colliders, and the powerful use one can make of this environment, is discussed in some detail in Gary Feldman's lectures at this school.^[11] On the other hand, e^+e^- colliders are well known to suffer one significant disadvantage:

The basic magnitude of all cross sections, familiar and exotic, is set by the point cross section

$$1R = \frac{4\pi\alpha^2}{3s} = \frac{86.8 \text{ fb}}{(E_{\text{CM}}(\text{TeV}))^2}. \quad (1.9)$$

That is, *all cross sections are small.*

To give a more concrete idea of the problem, let us compare the situation of a future e^+e^- collider to that of PEP. At PEP, the experiments to search for new particles were essentially complete after an integrated luminosity of 50 pb^{-1} . At $E_{\text{CM}} = 29 \text{ GeV}$, this corresponds to 5000 R^{-1} . The data sample corresponds to 10^7 sec running with a luminosity of $5 \times 10^{30} \text{ cm}^{-2}\text{sec}^{-1}$. The analogous data sample of 5000 R^{-1} at a 1 TeV linear collider would require 10^7 sec running with a luminosity of $5 \times 10^{33} \text{ cm}^{-2}\text{sec}^{-1}$. This poses a severe constraint on the design of future colliders. However, accelerator physicists at SLAC and CERN have recently expressed optimism about designing machines with luminosities of $3 \times 10^{33} \text{ cm}^{-2}\text{sec}^{-1}$ and above. For the remainder of these lectures, I will share their optimism that such colliders can be built. The technical problems of machine design which must be addressed are discussed further in Gary Feldman's lectures.

In these lectures, I will concentrate on setting out the various reactions which might produce new physics at a TeV-energy linear e^+e^- collider and on reporting the cross sections and general characteristics expected for these processes. I will proceed as follows: I will begin in Section 2 by discussing the standard model at TeV energies, reviewing the various fermion and boson pair-production processes which are expected to be the most important standard processes at a new e^+e^- collider. In Section 3, I will discuss the pair-production of new fermions and bosons, and some searches for new physics involving reactions of the standard model. In Section 4, I will describe the properties of new Z^0 bosons as they would be seen by a high-energy e^+e^- collider. Finally, in Section 5, I will review the physics of Higgs and W bosons at high energy and explain how the Higgs mechanism of

vector boson mass generation manifests itself experimentally. Section 6 presents some conclusions.

Throughout these lectures, I will adhere to two conventions which reflect the major themes of my presentation. First, since all of the processes I will discuss have cross sections of the order of the point cross section (1.9), I will quote all cross sections in units of R . This will immediately allow one to assess the importance of each particular reaction relative to other modes of e^+e^- annihilation. The conversion to more standard units can be made directly using (1.9). Second, I will, wherever possible, quote polarized cross sections taken between states of definite helicity rather than simply polarization-averaged cross sections. In these lectures, we will be discussing physics in the regime well above the W mass, where the weak interactions are as important as the electromagnetic interactions. In this regime, the left- and right-handed electrons, and the helicity states of other matter fermions, behave like distinct species. We should be prepared to find large polarization effects which can be characteristic signatures of old and new reactions.

2. Standard Model Processes

Let us begin by describing the most important processes of the standard model which would appear at a TeV-energy e^+e^- collider. These processes are of some interest in their own right; in addition, they provide the dominant background processes for particle search experiments. For the most part, we can argue about these high energies by smoothly extending the familiar results from currently available energies. But there is an important new feature, the emergence of reactions involving the pair-production of weak vector bosons. At $E_{CM} = 1$ TeV, the pair-production of W bosons is the most important single component of the e^+e^- annihilation cross section.

2.1. PERIPHERAL PROCESSES

The two most prominent processes at high-energy e^+e^- colliders are those already familiar from current experiments—Bhabha scattering and two-photon pair-production reactions. Bhabha scattering ($e^+e^- \rightarrow e^+e^-$) is well known to have a differential cross section which diverges in the forward direction and settles down to a value of a few R at wide angles. I will present explicit formulae for the cross section in my discussion of electron compositeness, Section 3.3.

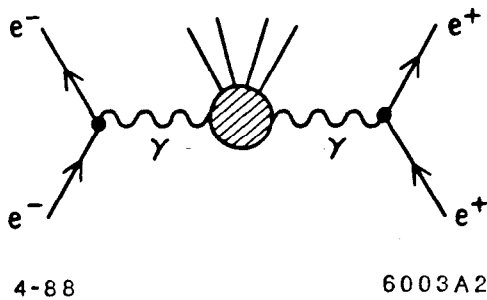


Figure 2. The two photon process.

The two-photon process involves the creation of fermion pairs from virtual photons emitted by the colliding electron and positron (Fig. 2). For our purposes, the main feature of this reaction is that it is readily distinguished kinematically from annihilation processes. The cross section is quite small, both in terms of the absolute rate it provides to a detector and in terms of the background it implies for relatively large invariant masses of the produced system. Estimating the rate at $\sqrt{s} = 1$ TeV using a Weizsacker-Williams spectrum for each photon, one finds for low invariant masses^[6]

$$\sigma(e^+e^- \rightarrow e^+e^-q\bar{q}) \sim \begin{cases} 100\text{nb} & |p_\perp| > 1 \text{ GeV} \\ 0.5\text{nb} & |p_\perp| > 10 \text{ GeV} \end{cases}, \quad (2.1)$$

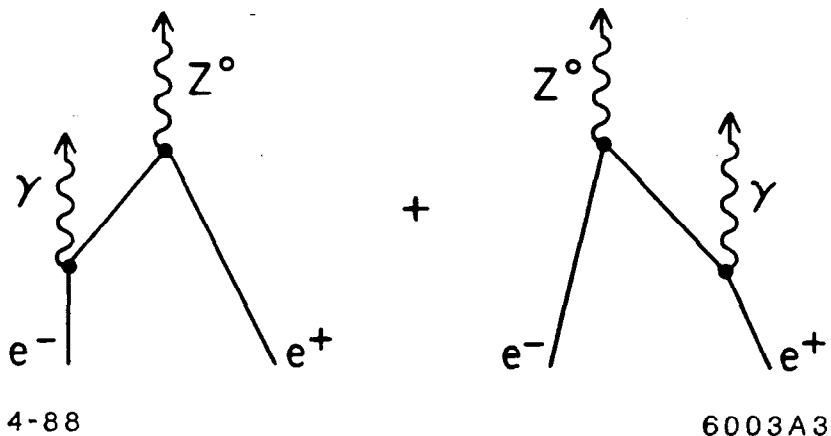


Figure 3. Collinear photon radiation to the Z^0 resonance.

and for high invariant masses

$$\sigma(e^+e^- \rightarrow e^+e^-q\bar{q}) \sim \begin{cases} 500R & |p_\perp| > 25 \text{ GeV} \\ 5R & |p_\perp| > 100 \text{ GeV} \end{cases} . \quad (2.2)$$

Since the final states which would be detected are simply pairs of quark jets, this process is not an important background to searches for new, heavy states.

At very high energies, pair-production of two photons and other pairs of vector bosons can also have large forward peaks. The reaction involving photons are cleanly distinguishable from new physics; the other reactions of this type are mainly interesting away from the forward direction. I will discuss their general characteristics in Section 2.3. However, I should note one interesting feature here. In the part of phase space for $e^+e^- \rightarrow \gamma Z^0$ in which the photon is emitted directly forward (Fig. 3), the electron stays close to its mass shell and the cross section for Z^0 production is enormously increased. By taking the photon from a Weizsäcker-Williams distribution, or simply by integrating the cross section for γZ^0 production over forward angles, one finds (in units of R , eq. (1.9))

$$-\overline{\sigma}(e^+e^- \rightarrow \gamma Z^0) \cong 3 \cdot \left[\frac{(\frac{1}{2} - \sin^2 \theta_w)^2 + (\sin^2 \theta_w)^2}{2 \sin^2 \theta_w \cos^2 \theta_w} \right] \cdot \frac{1 + m_Z^2/s^2}{(1 - m_Z^2/s)} \cdot \log\left(\frac{s}{m_e^2}\right) \quad (2.3)$$

This corresponds to 31 units of R at $\sqrt{s} = 1$ TeV. Essentially all the Z^0 bosons are emitted with a substantial boost along the beam axis: $\gamma(Z^0) = 11$. Fortunately or unfortunately, it is difficult to imagine that many of these Z^0 bosons would be well reconstructed.

2.2. FERMION PAIR-PRODUCTION

The study of e^+e^- annihilation into fermion pairs is the bread and butter of electron-positron collider experiments at current energies, and this process will remain an important one at TeV energies. The main new feature is that the two diagrams with a photon and a Z^0 in the s -channel (Fig. 4) now compete on the same footing, giving rise to large forward-backward and polarization asymmetries. The cross section for this process is most simply written in terms of helicity states;

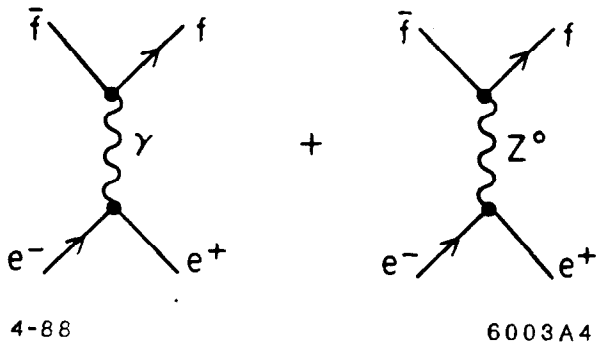


Figure 4. Diagrams contributing to e^+e^- annihilation to fermion pairs.

an elementary process would then be a reaction $e_L^- e_R^+ \rightarrow q_L \bar{q}_R$. By helicity conservation, left-handed particles annihilate only right-handed antiparticles, and vice versa. The two nonzero cross sections from states of definite helicity are

$$\begin{aligned} \frac{d\sigma}{d\cos\theta}(e_L^- e_R^+ \rightarrow f\bar{f}) &= \frac{3}{8} N_c \{ |f_{LL}|^2 \cdot (1 + \cos\theta)^2 + |f_{LR}|^2 \cdot (1 - \cos\theta)^2 \} \\ \frac{-d\sigma}{d\cos\theta}(e_R^- e_L^+ \rightarrow f\bar{f}) &= \frac{3}{8} N_c \{ |f_{RR}|^2 \cdot (1 + \cos\theta)^2 + |f_{RL}|^2 \cdot (1 - \cos\theta)^2 \} . \end{aligned} \quad (2.4)$$

Again, the cross sections are expressed in R units. The quantity f_{LR} is the amplitude for a left-handed electron to annihilate to a right-handed quark or lepton, plus its antiparticle, and the other amplitudes f are defined similarly. Explicitly, for fermion generations of the standard form,

$$\begin{aligned}
 f_{LL} &= -Q + \frac{(-\frac{1}{2} + \sin^2 \theta_w)(I^3 - Q \sin^2 \theta_w)}{\sin^2 \theta_w \cos^2 \theta_w} \frac{s}{s - m_Z^2} \\
 f_{RL} &= -Q + \frac{(\sin^2 \theta_w)(I^3 - Q \sin^2 \theta_w)}{\sin^2 \theta_w \cos^2 \theta_w} \frac{s}{s - m_Z^2} \\
 f_{LR} &= -Q + \frac{(-\frac{1}{2} + \sin^2 \theta_w)(-Q \sin^2 \theta_w)}{\sin^2 \theta_w \cos^2 \theta_w} \frac{s}{s - m_Z^2} \\
 f_{RR} &= -Q + \frac{(\sin^2 \theta_w)(-Q \sin^2 \theta_w)}{\sin^2 \theta_w \cos^2 \theta_w} \frac{s}{s - m_Z^2}.
 \end{aligned} \tag{2.5}$$

The factor N_c accounts the number of colors and the QCD correction to the cross section; it is

$$N_c = \begin{cases} 1 & \text{for leptons} \\ 3 \cdot (1 + \frac{\alpha_s}{\pi} + \dots) & \text{for quarks} \end{cases} \tag{2.6}$$

Because (2.4) has such a simple dependence on $\cos \theta$, the amplitudes f can be directly converted into the basic integral measures which characterize the process of fermion pair-production. The total cross section from unpolarized beams is given by

$$\sigma_{\text{tot}} = \frac{1}{4} [|f_{LL}|^2 + |f_{LR}|^2 + |f_{RL}|^2 + |f_{RR}|^2]. \tag{2.7}$$

For the purposes of this talk, I will define the forward-backward asymmetry using a theorist's notion that one can integrate over all solid angles. Then this asymmetry

is given by

$$\begin{aligned}
 A_{FB} &= \frac{\int_{\cos \theta > 0} - \int_{\cos \theta < 0} d \cos \theta \frac{(d\sigma/d \cos \theta)}{d \cos \theta}}{\int_{\cos \theta > 0} + \int_{\cos \theta < 0} d \cos \theta \frac{(d\sigma/d \cos \theta)}{d \cos \theta}} \\
 &= (0.75) \frac{(|f_{LL}|^2 + |f_{RR}|^2) - (|f_{LR}|^2 + |f_{RL}|^2)}{|f_{LL}|^2 + |f_{RR}|^2 + |f_{LR}|^2 + |f_{RL}|^2} \quad (2.8)
 \end{aligned}$$

Finally, the polarization asymmetry is

$$\begin{aligned}
 A_{\text{pol}} &= \frac{\sigma(e_L^- e^+ \rightarrow f\bar{f}) - \sigma(e_R^- e^+ \rightarrow f\bar{f})}{\sigma(e_L^- e^+ \rightarrow f\bar{f}) + \sigma(e_R^- e^+ \rightarrow f\bar{f})} \\
 &= \frac{(|f_{LL}|^2 + |f_{LR}|^2) - (|f_{RL}|^2 + |f_{RR}|^2)}{|f_{LL}|^2 + |f_{LR}|^2 + |f_{RL}|^2 + |f_{RR}|^2} \quad (2.9)
 \end{aligned}$$

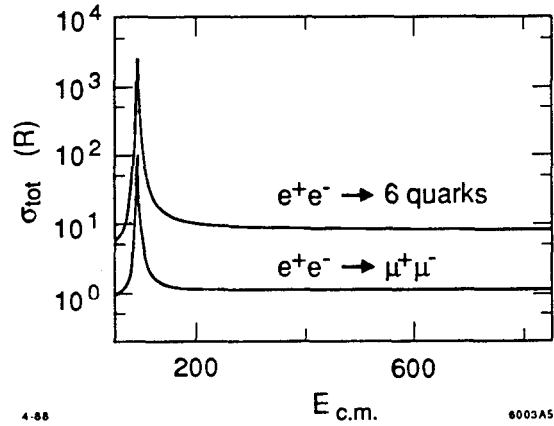


Figure 5. Total cross section for $e^+e^- \rightarrow \mu^+\mu^-$ and $e^+e^- \rightarrow q\bar{q}$, assuming six light quarks.

Figures 5, 6, and 7 illustrate some properties of these formulae in the regime well above the Z^0 . Figure 5 shows the total cross section to μ pairs and to all quark pairs. (The cross sections are given in units of R ; note that the μ pair cross section

is slightly greater than 1 R due to the contribution of the Z^0 .) The asymptotic

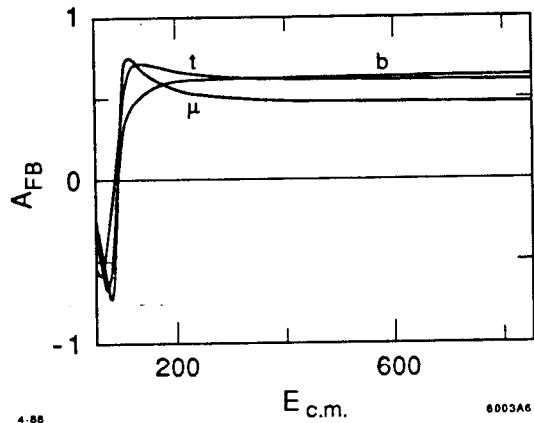


Figure 6. Forward-backward asymmetry for the production of μ , b and t pairs.

total cross section for quark pair-production is 8.5 R. Figure 6 shows the forward-backward asymmetry for the three species for which it is most easily measured— μ , b , and t . Figure 7 shows the polarization asymmetry for production of these three

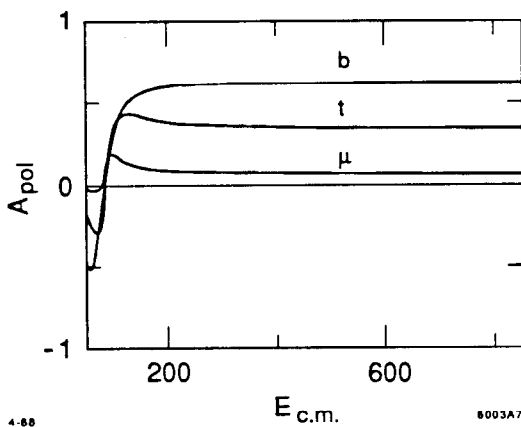


Figure 7. Polarization asymmetry for the production of μ , b , and t pairs.

species. If the t quark is relatively light, it may be difficult to separate the $t\bar{t}$ and $b\bar{b}$ events, especially since t quarks are expected to rapidly decay to b quarks. In that case, it is worth noting that the contributions of t and b to the forward-backward asymmetry can substantially cancel if the quark direction is measured as the direction of a charged lepton from a semileptonic decay. However, the contributions of t and b to the polarization asymmetry always add. Even assuming maximal confusion, we have

$$A_{FB}(t-b) = 0.18, \quad A_{\text{pol}}(t+b) = 0.44. \quad (2.10)$$

The asymptotic values of the total cross sections and asymmetries for the basic fermion species of the standard model are summarized in Table 2. In addition to the features noted in the previous paragraph, there is one more which is of importance. Due to the Z^0 diagram, the cross section for producing neutrino pairs is substantial. For three generations,

$$\sigma(e^+e^- \rightarrow \nu\bar{\nu}) = 0.75 \text{ R}. \quad (2.11)$$

This is a large background to searches for e^+e^- annihilation into completely invisible final states.

Table 2: Properties of e^+e^- annihilation into fermion pairs for $s \gg m_Z^2$

	<u>σ_{tot}</u>	<u>A_{FB}</u>	<u>A_{pol}</u>
u	1.86	0.60	0.34
d	0.96	0.64	0.62
ℓ^-	1.13	0.47	0.07
ν	0.25	0.12	0.15

2.3. VECTOR BOSON PAIR-PRODUCTION

At center-of-mass energies well above m_W , the weak vector bosons behave as light elementary states, on the same footing as the photon. It is therefore easy to understand that these particles might have very large pair-production cross sections. In fact, these vector boson pair-production reactions become some of the largest components of the total e^+e^- annihilation cross section.

To understand the size of these processes, it is simplest to begin with a very well known reaction, $e^+e^- \rightarrow \gamma\gamma$. The lowest-order Feynman diagrams for this process are shown in Fig. 8. These diagrams lead to the following expression for

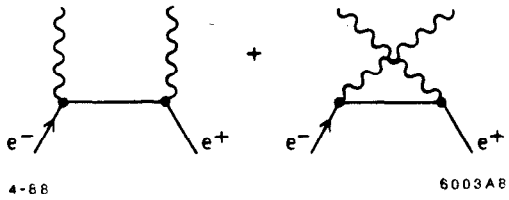


Figure 8. Feynman diagrams for e^+e^- annihilation into neutral vector bosons:
 $e^+e^- \rightarrow \gamma\gamma, Z^0\gamma, Z^0Z^0$.

the differential cross section (as always, in units of R)

$$\frac{d\sigma}{d\cos\theta} = \frac{3}{4} \left(\frac{u}{t} + \frac{t}{u} \right), \quad (2.12)$$

where

$$t = -\frac{1}{2}s(1 - \cos\theta) \quad u = -\frac{1}{2}s(1 + \cos\theta). \quad (2.13)$$

This formula is averaged over electron polarization states, but it receives equal contributions from $e_L^-e_R^+$ and $e_R^-e_L^+$ annihilation. Because photons are identical particles, the total cross section is obtained by integrating (2.12) over $\cos\theta > 0$ only.

Since the production of $Z^0\gamma$ and Z^0 pairs involves just the same two Feynman diagrams, these cross sections may be estimated straightforwardly by multiplying (2.12) by the appropriate factors of $\sin^2 \theta_w$ to give the electron coupling to the Z^0 for each of the two possible electron helicities. To determine the precise cross sections, one must also work out the dependence on m_Z .^[12] For $e^+e^- \rightarrow Z^0\gamma$, the differential cross section from unpolarized electrons and positrons is given by

$$\frac{d\sigma}{d\cos\theta} = \frac{3}{4} \cdot \frac{(\frac{1}{2} - \sin^2 \theta_w)^2 + (\sin^2 \theta_w)^2}{2 \sin^2 \theta_w \cos^2 \theta_w} \cdot \left(1 - \frac{m_Z^2}{s}\right) \cdot \left\{ \frac{(u - m_Z^2)^2 + (t - m_Z^2)^2}{ut} \right\}, \quad (2.14)$$

where

$$t = -\frac{1}{2}(s - m_Z^2)(1 - \cos\theta), \quad u = -\frac{1}{2}(s - m_Z^2)(1 + \cos\theta). \quad (2.15)$$

This formula may be integrated over all values of $\cos\theta$. For $e^+e^- \rightarrow Z^0Z^0$, the differential cross section from unpolarized electrons and positrons is

$$\frac{d\sigma}{d\cos\theta} = \frac{3}{4} \cdot \frac{(\frac{1}{2} - \sin^2 \theta_w)^4 + (\sin^2 \theta_w)^4}{2 \sin^4 \theta_w \cos^4 \theta_w} \cdot \left(1 - \frac{4m_Z^2}{s}\right)^{1/2} \cdot \left\{ \frac{u}{t} + \frac{t}{u} + 4m_Z^2 \frac{s}{ut} - m_Z^4 \left(\frac{1}{u^2} + \frac{1}{t^2}\right) \right\}, \quad (2.16)$$

where

$$\begin{aligned} t &= -\frac{1}{2}(s - (s(s - 4m_Z^2))^{1/2} \cos\theta) + m_Z^2, \\ u &= -\frac{1}{2}(s + (s(s - 4m_Z^2))^{1/2} \cos\theta) + m_Z^2. \end{aligned} \quad (2.17)$$

This formula should be integrated only over $\cos\theta > 0$. The final boson pair-production process, $e^+e^- \rightarrow W^+W^-$, has a considerably more complicated structure.^[13,14] I will postpone my discussion of this reaction to Section 5.3.

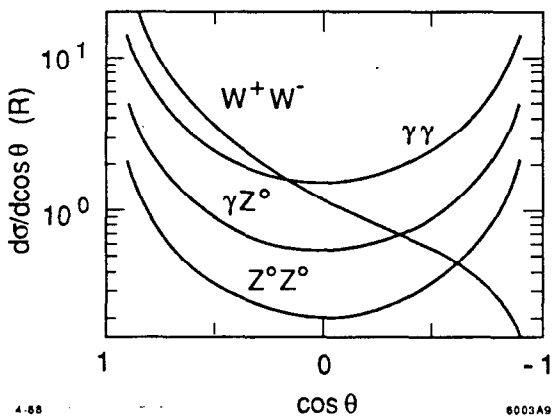


Figure 9. Differential cross sections for e^+e^- annihilation into two vector bosons.

The four differential cross sections for boson pair-production are shown in Fig. 9. The three new processes are comparable in size to $e^+e^- \rightarrow \gamma\gamma$, and actually the W pair-production process is somewhat larger. All four processes have large forward peaks, generated by the t channel exchange of electrons (or, for W production, neutrinos). For the W^+W^- and Z^0Z^0 reactions, this forward peak is eventually cut off by the W mass, producing a finite cross section of order (for W pairs) $25 R$ at 1 TeV. I have already noted that the $Z^0\gamma$ reaction is cut off only by the electron mass; indeed, one can recover the formula (2.3) for forward Z^0 production by integrating (2.14) over its forward and backward peaks.

3. New Particles and Couplings

I have argued in Section 1 that, in the energy region near 1 TeV, we should expect the standard model to be supplemented by a rich array of new particles. The search for these particles will be the major task of a high energy e^+e^- collider, and the discovery of such new particles will shed important light on the mechanism of the weak interaction gauge symmetry breaking.

For the most part, the theory of the production of these new particles is very simple: The new states are pair-produced in just the same way as the familiar

particles of the standard model. In this section, I will present a sampler of hypothesized states and discuss some other basic experiments which bear on the physics of the TeV scale.

3.1. NEW FERMIONS

One obvious possibility, as we probe to higher energies, is that we will discover further generations of quarks and leptons. If these fermions have the quantum numbers of members of standard generations, their production characteristics follow exactly the discussion of Section 2.2. The main difference between these heavier fermions and conventional ones comes in their pattern of decay. If $m_Q > m_W$, so that the heavy quark can decay to an on-shell W boson, this decay mode becomes dominant. The corresponding width is decay is

$$\Gamma(Q \rightarrow Wq) = \frac{\alpha M}{16 \sin^2 \theta_w} \cdot \left(\frac{M}{m_W} \right)^2 \cdot \left(1 + 2 \frac{m_W^2}{M^2} \right) \cdot \left(1 - \frac{m_W^2}{M^2} \right)^2, \quad (3.1)$$

times generalized Cabibbo mixing angles. Gary Feldman will discuss the practical importance of this decay mode: At an e^+e^- collider, the W in the final state can be reconstructed by combining jets identified calorimetrically. Thus, the signature of a heavy quark is a striking one, and the heavy quark events should be easy to isolate.^[11]

If new heavy quarks exist, how heavy should they be? A priori, the standard model gives little concrete information constraining these masses, but there are two milestones which set the general scale. The first of these comes from the observation of Pendleton and Ross,^[15] and Hill^[16] that there is a fixed point in the renormalization of the quark-Higgs boson coupling λ_q (eq. (1.6)). If λ_q is small, the QCD renormalization tends to increase it at larger distances, but if λ_q is large, effects nonlinear in λ_q tend to decrease it. The precise evolution equation

(at one-loop order) for a heavy-charge ($\frac{2}{3}$) quark is

$$\frac{d\lambda_U}{d \log r} = \lambda_U \cdot \left[+ 8g_s^2 + \frac{9}{4}g^2 + \frac{17}{20}g'^2 - 3\text{tr}(\lambda_U^\dagger \lambda_U + \lambda_D^\dagger \lambda_D) - \frac{3}{2}(\lambda_U^\dagger \lambda_U - \lambda_D^\dagger \lambda_D) \right]; \quad (3.2)$$

a similar equation applies for λ_D . If quark-Higgs coupling constants are randomly distributed at the scale of grand unification, their renormalization down to the weak interaction scale tends to drive them to the point of balance between these two renormalization effects, that is, toward the value

$$\lambda_U \approx \lambda_D \approx \frac{4}{3}g_s^2/\sqrt{N_H} \sim \frac{1.8}{\sqrt{N_H}}, \quad (3.3)$$

where N_H is the number of heavy generations accumulating at this point. This corresponds to quark masses of

$$m_U \approx m_D \sim 300 \text{ GeV}/\sqrt{N_H}. \quad (3.4)$$

Note that the u and d quark masses within the heavy generations become closely degenerate. Bagger, Dimopoulos, and Massó^[17] have studied the rate of evolution and confirmed that the flow toward this fixed point is fast enough that we might expect convergence of one—or possibly several—new generations to within about 20% of the fixed point value. Figure 10 illustrates the convergence of couplings λ_q which they have observed.

The second milestone comes from the observation that, as the mass of the new quark becomes very heavy, the coupling λ_q must increase to the point where the quark-Higgs system becomes strongly coupled. Chanowitz, Furman, and Hinchliffe^[18] have noted that one has entered this strong-coupling regime at the point at which the lowest-order S -matrix elements for quark-quark scattering due to Higgs

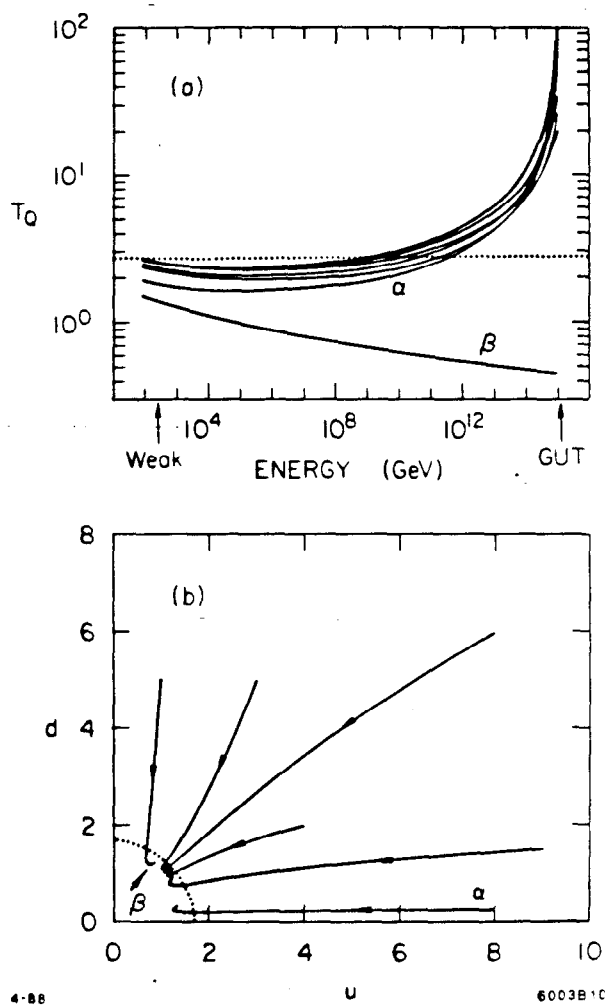


Figure 10. Renormalization-group flows of quark-Higgs boson coupling constants, according to Ref. 17: (a) evolution of the magnitude of λ_q for various initial conditions at the grand unification scale; (b) evolution of the u to d quark mass ratio in a heavy generation.

exchange becomes so large as to violate unitarity. They showed that this point occurs at

$$m_Q = \frac{4\sqrt{2}\pi}{5G_F} = 550 \text{ GeV} . \quad (3.5)$$

This value actually need not be an upper bound to quark masses in the standard model; above this mass, models with heavy quarks merge smoothly into technicolor

models. But the calculation does indicate that we may find heavy quarks, relatively decoupled from the weak symmetry breaking sector, all the way up to this rather high scale.

In addition to further standard generations, we might expect to find fermions with nonstandard electroweak quantum numbers. Many varieties of weak-interaction models contain additional ('mirror') generations with $(V+A)$ rather than $(V-A)$ coupling to the W and similarly parity-conjugate couplings to the Z^0 . (Two disparate examples, are given in Refs. 19, 20.) Theories which produce new Z^0 bosons often contain additional fermions which receive mass when the extended gauge symmetry is broken. The class of theories discussed in Section 4, for example, can contain a charge $(-\frac{1}{3})$ quark D which is neutral under weak interactions and a lepton doublet (N, E) with vectorlike weak interactions. The basic integral quantities for e^+e^- annihilation to these states are given in Table 3.

Table 3: Properties of e^+e^- annihilation into fermion pairs with nonstandard weak quantum numbers

		<u>σ_{tot}</u>	<u>A_{FB}</u>	<u>A_{pol}</u>
mirror	u	1.86	-0.60	0.34
	d	0.96	-0.63	0.62
	ℓ^-	1.13	-0.47	0.67
vectorlike	D	0.36	0	-0.60
	N	0.50	0	0.16
	E	1.21	0	0.65

It is worth comparing the entries in this table to those in Table 2; some differences are striking. For example, the vectorlike D quark has a polarization asymmetry which is large and opposite in sign to that for a standard d . The substantial forward-backward asymmetries for ordinary quarks flip sign for mirror generations. These obvious features should be readily observable when the new states are pair-produced at an e^+e^- collider.

3.2. NEW SECTORS OF BOSONS

Beyond the question of identifying new fermions, we can hope that TeV energy experiments will reveal a rich sector of particles which form the mechanics of the $SU(2) \times U(1)$ symmetry breaking. Issues arising directly from the interplay of symmetry breaking, Higgs bosons, and W bosons will be discussed separately in Section 5. But, as I have noted in Section 1.1, mechanical models of weak interaction symmetry breaking are often complex, with intricately arranged spectra of new particles. In this section, I would like to discuss the two most prominent classes of such models, models based on the ideas of supersymmetry and technicolor. I do not have space here for a detailed review of these ideas, but, in any event, this is hardly necessary, since there are excellent general reviews of these theoretical schemes. For supersymmetry, the basic structure of the phenomenological theory has been set out in Refs. 21–23 and the signatures in e^+e^- annihilation have been discussed in some detail by Barnett at a previous session of this school.^[24] The basic principles and phenomena of technicolor theories have been explained in Refs. 25–27. In this section, I would like simply to recall the basic principles of these theoretical constructions and the particular new particles they predict which would give the most prominent signatures at an e^+e^- collider.

The basic idea of supersymmetry is the postulate of a fundamental space-time symmetry linking fermion and boson states. Its main prediction is the doubling of the spectrum of fundamental particles—for each known fermion, we expect a bosonic partner, for each known boson, a fermion. In all cases, there are good theoretical reasons why the partner which is familiar to us should be the lighter of the two. However, the heavier partners can be no heavier than the mass scale of supersymmetry breaking. If this is linked with the weak scale, we expect all of the undiscovered partners to appear below energies of about 1 TeV. The spectrum of a realistic supersymmetric extension of the standard model, taken at a random point in its parameter space, is shown in Fig. 11. Note that the scalar partners of the leptons, u quarks, and d quarks in the lighter generations are expected to

be almost degenerate; however, the scalar partners of the left- and right-handed species may have substantially different masses. The fermionic partners of gauge and Higgs bosons are expected to mix strongly; it has become common to label these mixed states as simply 'neutralinos' and 'charginos'.

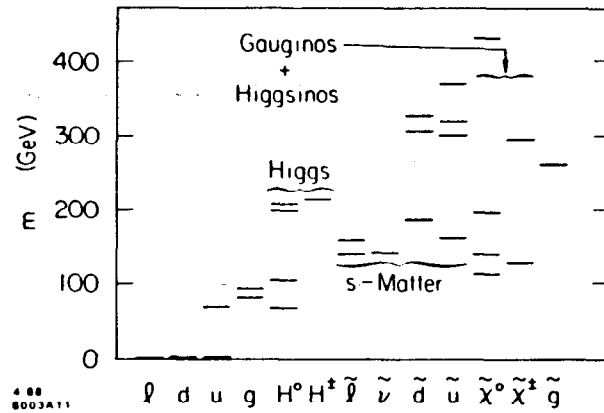


Figure 11. Spectrum of a supersymmetric model of the strong, weak, and electromagnetic interactions, taken at an arbitrarily chosen set of its parameters (from Ref. 28).

If the mass scale of fermion superpartners is relatively low, the pair-production of these partners would be a prominent contribution to the e^+e^- annihilation cross section. These states should decay characteristically to their fermionic partners plus (unobserved, penetrating) neutralinos. The pair-production cross section for these scalars from longitudinally polarized beams is readily computed to be

$$\begin{aligned} \frac{d\sigma}{d\cos\theta} (e_L^- e_R^+ \rightarrow \tilde{f} \tilde{\bar{f}}) &= \frac{3}{8} N_c \cdot |f_L|^2 \sin^2\theta \\ \frac{d\sigma}{d\cos\theta} (e_R^- e_L^+ \rightarrow \tilde{f} \tilde{\bar{f}}) &= \frac{3}{8} N_c \cdot |f_R|^2 \sin^2\theta. \end{aligned} \quad (3.6)$$

The amplitudes f are given by

$$\begin{aligned} f_L &= -Q + \frac{(-\frac{1}{2} + \sin^2 \theta_w) Q_Z}{\sin^2 \theta_w \cos^2 \theta_w} \frac{s}{s - m_z^2} \\ f_R &= -Q + \frac{(\sin^2 \theta_w) Q_Z}{\sin^2 \theta_w \cos^2 \theta_w} \frac{s}{s - m_z^2} , \end{aligned} \quad (3.7)$$

where, for squarks and sleptons

$$Q_Z = I_L^3 - Q \sin^2 \theta_w . \quad (3.8)$$

Here I_L^3 is the weak interaction quantum number, equal to $(-\frac{1}{2})$, for example, for the partner of e_L^- and to 0 for the partner of e_R^- . The color factor is

$$N_c = \begin{cases} 1 & \text{for sleptons} \\ 3 \cdot (1 + \frac{4\alpha_s}{\pi} + \dots) & \text{for squarks} \end{cases} \quad (3.9)$$

Table 4: Properties of e^+e^- annihilation into supersymmetric partners of quarks and leptons

	σ_{tot}	A_{pol}
\tilde{u}_L	0.63	0.94
\tilde{u}_R	0.40	-0.60
\tilde{d}_L	0.43	0.91
\tilde{d}_R	0.10	-0.60
$\tilde{\ell}_L$	0.30	0.65
$\tilde{\ell}_R$	0.26	-0.60
$\tilde{\nu}$	0.13	0.16

As a matter of principle, scalars cannot have a forward-backward asymmetry; the other two integral quantities can be computed from the amplitudes f as indicated in (2.7), (2.12). The expected values of the total cross sections and polarization asymmetries for superpartners of matter fermions are shown in Table

4. In assessing the total cross sections, one should recall that the thresholds for two and possibly three generations of each species should be very close together. A striking feature of the information in this table is the wide variation of the polarization asymmetry. The superpartners of the left- and right-handed quarks, for example, have polarization asymmetries with large values and the opposite signs. The feature can probably be used to measure the mass difference between the two squarks of each charge.

At the other extreme, let us consider the case in which the mass scale of supersymmetry is relatively high. In this case, the first sign of the presence of supersymmetry might come from the pair-production of neutralinos, since these are normally the lightest supersymmetric states. Let us label the two lightest neutralinos as $\tilde{\chi}_1, \tilde{\chi}_2$. The $\tilde{\chi}_1$, as the lightest superpartner, is likely to be absolutely stable. In principle, one could search for the pair-production of $\tilde{\chi}_1$; however, this would be very difficult because the substantial process of neutrino pair-production is a background. A more promising reactions is the process

$$e^+e^- \rightarrow \tilde{\chi}_1\tilde{\chi}_2 . \quad (3.10)$$

The Feynman diagrams contributing to this reaction are shown in Fig. 12. The precise expression for the cross-section is complex and model-dependent, since it contains the mixing angles which parametrize the $\tilde{\chi}$ mass eigenstates. However,

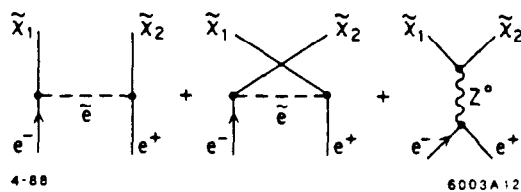


Figure 12. Contributions to the cross section for the production of neutralinos through $e^+e^- \rightarrow \tilde{\chi}_1\tilde{\chi}_2$.

one can say generally that the \tilde{e} exchange diagrams dominate unless $m_{\tilde{e}} >> 1$ TeV and that, for $m_{\tilde{e}} \sim 1$ TeV, the total cross section for this process is of order 0.1 R. The signature can be striking: The $\tilde{\chi}_1$ should be unobserved, and the $\tilde{\chi}_2$ should decay according to

$$\tilde{\chi}_2 \rightarrow \tilde{\chi}_1 + \{ f\bar{f}, Z^0, H^0, \dots \}, \quad (3.11)$$

producing events with single, weakly interacting states ejected at large transverse momentum.^[29]

The basic idea of technicolor is the postulate of a new set of strong interactions in the form of a gauge theory of fermions and gauge bosons. The expectation is that this theory would have chiral symmetry breaking and spontaneous fermion mass generation in just the manner of the familiar strong interactions. If the new fermions have the weak quantum numbers of a standard generation, this process can then be shown to break $SU(2) \times U(1)$ spontaneously in just the manner required for the standard model. Potentially, this model gives rise to many new states, called ‘technipions’, which one might think of either as composite Higgs bosons built of the new fermions or as the pions and kaons associated with the new strong interactions. Normally, at least one charged scalar is expected to appear, and scalar particles with more exotic quantum numbers—for example, color octet scalars or scalars with lepton-quark quantum numbers—are also possible. Though these particles are composite, they are small; as long as we remain well below the energy scale of the new strong interactions, we can treat them, in their coupling to the weak and electromagnetic interactions, as pointlike elementary particles. In that case, their cross sections for pair-production are again given by (3.6), (3.7). The weak charges Q_Z are given by

$$Q_Z = I^3 - 2Q \sin^2 \theta_w, \quad (3.12)$$

where I^3 is the vector isospin and Q is the electric charge. In general, the coupling of a pair of such composite scalars to a gauge boson is given by the vector part of

the gauge current. The color factor N_c is

$$N_c = \begin{cases} 1 & \text{for color singlets} \\ 3 \cdot \left(1 + \frac{4\alpha_s}{\pi} + \dots\right) & \text{for color triplets} \\ 8 \cdot \left(1 + \frac{9\alpha_s}{\pi} + \dots\right) & \text{for color octets} \end{cases} \quad (3.13)$$

The total cross sections and polarization asymmetries for a variety of composite scalars are compiled in Table 5.

Table 5: Properties of e^+e^- annihilation into pairs of technicolor bosons

		<u>σ_{tot}</u>	<u>A_{pol}</u>
charged Higgs	H^\pm	0.3	0.65
color 8	H^\pm	3.0	0.65
leptoquarks	$(\bar{E}U)$	2.6	0.48
	$(\bar{E}U)$	0.4	0.31
	$(\bar{N}U)$	0.4	0.31
	$(\bar{N}D)$	0.5	0.88

Though some models of technicolor place the new strong interactions at a mass scale of 2 TeV or higher, other models have new resonance structure at a relatively low energy. Farhi and Susskind^[30] have introduced models with especially rich spectra of technipions, and in these models, the technicolor analogue of the rho meson has a mass of 900 GeV. This meson manifests itself experimentally as a resonant enhancement in technipion production—a striking effect on the cross section for e^+e^- annihilation into heavy states. The form of the technipion cross sections expected in the neighborhood of the techni-rho is shown in Fig. 13.^[6]

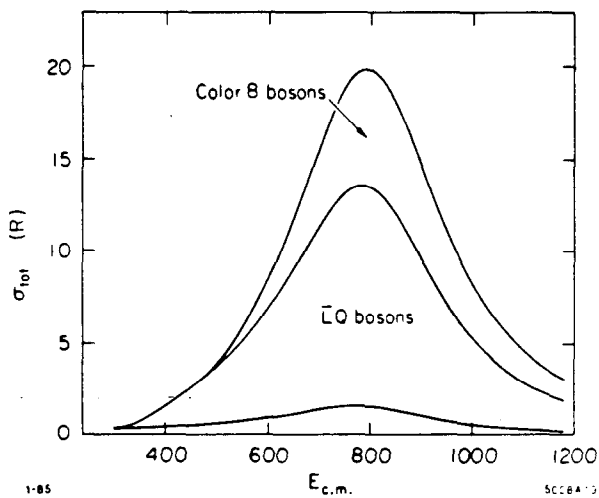


Figure 13. Resonant enhancement of composite Higgs boson production due to the presence of the rho meson of technicolor strong interactions.

3.3. LEPTON SUBSTRUCTURE

In addition to searching for exotic reactions, it will be an important task for physicists at a high energy collider to measure the conventional reactions of the standard model with high precision. In some cases, such precision measurements can be as telling as new particle searches in illuminating physics beyond the standard model. One further alternative for the direction which this physics might take is that quarks and leptons themselves might be composite states, with constituents bound at the energy scale of a few TeV. At the moment, the most stringent tests of this idea come from the detailed study of Bhabha scattering, and so one should expect that the study of Bhabha scattering at TeV energies might allow the discovery of lepton substructure.

The principle of the experiment is the following:^[31] If electrons are composite, they should be expected to possess new interactions beyond those of the standard model. These new interactions might arise from exchange of common constituents or, equivalently, exchange of vector mesons of the strong interactions responsible for constituent binding. The amplitude for Bhabha scattering is then given by

the sum of the Feynman diagrams shown in Fig. 14; the last diagram represents the new coupling. If the size of the composite leptons is very small, that is, if the

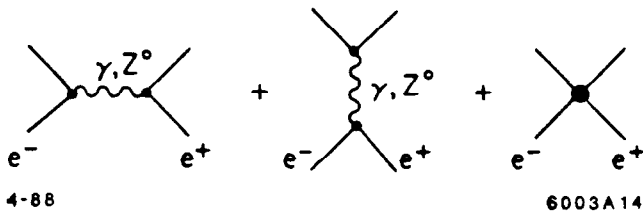


Figure 14. Contributions to the cross section for Bhabha scattering in a model with lepton substructure.

momentum scale of binding is very large relative to \sqrt{s} , the constituent exchange interaction can be approximated by a four-fermion contact interaction. Using helicity conservation, we can write any electron-electron contact interactions in the general form

$$\mathcal{L}_{\text{eff}} = \frac{g^2}{2\Lambda^2} \left[\eta_{LL} (\bar{e}_L \gamma^\mu e_L) (\bar{e}_L \gamma_\mu e_L) + \eta_{LR} (\bar{e}_R \gamma^\mu e_R) (\bar{e}_R \gamma_\mu e_R) + 2\eta_{LR} (\bar{e}_L \gamma^\mu e_L) (\bar{e}_R \gamma_\mu e_R) \right], \quad (3.14)$$

where Λ is the momentum scale of constituent-binding, g is a dimensionless effective coupling constant, and the η parameters are of order 1. One might think of Λ as the mass of the rho meson in these new interactions. Since the new forces are strong, it makes sense to use the familiar rho meson to estimate g ; let us write

$$\frac{g^2}{4\pi} \sim \frac{1}{2} \frac{g_\rho^2}{4\pi} \sim 1. \quad (3.15)$$

Thus, though the contact interactions are suppressed by a large mass scale, they are enhanced as strong interactions competing with interactions of electromagnetic strength; further, the new effects can be seen as interference terms rather than

as competing reactions. This means that Bhabha scattering is extraordinarily sensitive to effects of electron compositeness; in fact, the current lower bounds on Λ from PEP and PETRA experiments are already of order 2 TeV.^[32]

Using (3.14) and (3.15), we can write the the differential cross section for Bhabha scattering of longitudinally polarized beams as

$$\begin{aligned}\frac{d\sigma}{d\cos\theta}(e_L^-e_R^+) &= \frac{3}{2} [u^2 D_{LL} + t^2 D_{LR}(s)] \\ \frac{d\sigma}{d\cos\theta}(e_L^-e_L^+) &= \frac{3}{2} [s^2 D_{LR}(t)] \\ \frac{d\sigma}{d\cos\theta}(e_R^-e_L^+) &= \frac{3}{2} [u^2 D_{RR} + t^2 D_{LR}(s)] \\ \frac{d\sigma}{d\cos\theta}(e_R^-e_L^+) &= \frac{3}{2} [s^2 D_{LR}(t)],\end{aligned}\tag{3.16}$$

where

$$\begin{aligned}D_{LL} &= \frac{1}{s} + \frac{1}{t} + \frac{(\frac{1}{2} - \sin^2\theta_w)^2}{\sin^2\theta_w \cos^2\theta_w} \left(\frac{1}{s - m_Z^2} + \frac{1}{t - m_Z^2} \right) + \frac{2\eta_{LL}s}{\alpha\Lambda^2} \\ D_{RR} &= \frac{1}{s} + \frac{1}{t} + \frac{(\sin^2\theta_w)^2}{\sin^2\theta_w \cos^2\theta_w} \left(\frac{1}{s - m_Z^2} + \frac{1}{t - m_Z^2} \right) + \frac{2\eta_{RR}s}{\alpha\Lambda^2} \\ D_{LR}(s) &= \frac{1}{s} + \frac{(\frac{1}{2} - \sin^2\theta_w)(-\sin^2\theta_w)}{\sin^2\theta_w \cos^2\theta_w} \frac{1}{s - m_Z^2} + \frac{\eta_{LR}s}{\alpha\Lambda^2}.\end{aligned}\tag{3.17}$$

In practice, it will be difficult to create a polarized e^+ beam, so I will present numerical results for polarized e^- scattering from unpolarized e^+ . A measure of the sensitivity of the Bhabha scattering cross section to contact interactions is given by

$$\Delta = \frac{\frac{d\sigma}{d\Omega} - \left(\frac{d\sigma}{d\Omega}\right)_0}{\left(\frac{d\sigma}{d\Omega}\right)_0},\tag{3.18}$$

where the subscript 0 denotes the cross section computed in the standard model ($\Lambda^{-2} = 0$). It is no problem to normalize the measured cross section; the cross

section at large angles can simply be compared to the cross section in the forward peaks, which is never appreciably affected by short-distance physics. In Figs. 15–17, I have plotted Δ as a function of $\cos\theta$ for three choices of the parameters of the new interactions. The error bars on each graph reflect the expected statistical errors for an integrated luminosity of $10^{40} \text{ cm}^{-2}\text{sec}^{-1}$ (10^3 R^{-1}) at $\sqrt{s} = 1 \text{ TeV}$, based on 8 bins in $\cos\theta$. The first two cases correspond to the coupling of vector

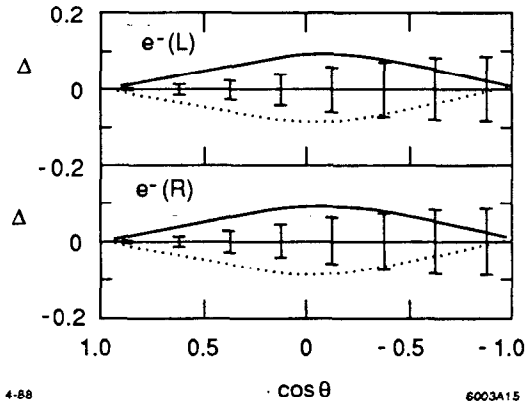


Figure 15. Observability of contact interactions in Bhabha scattering at $\sqrt{s} = 1 \text{ TeV}$, estimated for polarized e^- beams and an integrated luminosity of $10^{40} \text{ cm}^{-2}\text{sec}^{-1}$. The following parameter values were used: $\Lambda = 40 \text{ TeV}$, $\eta_{LL} = \eta_{RR} = \eta_{RL} = -1$. The dotted line shows the effect of changing the overall sign of the contact term.

currents (Fig. 15) and left-handed currents (Fig. 16). The third case is one devised by Schrempp as being particularly troublesome because of the cancellation of the leading contributions from the contact term. But note that the use of polarized electrons straightforwardly resolves this ambiguity.^[33] It seems clear, then, that a TeV e^+e^- collider would be sensitive to electron compositeness at the level of 50 TeV or beyond.

An important property of the formulae (3.17) is that the effect of contact interactions increases with s . Eventually, when the reaction energy reaches the scale Λ , we expect to see geometrical cross sections: $\sigma \sim \Lambda^{-2}$. This means that, if

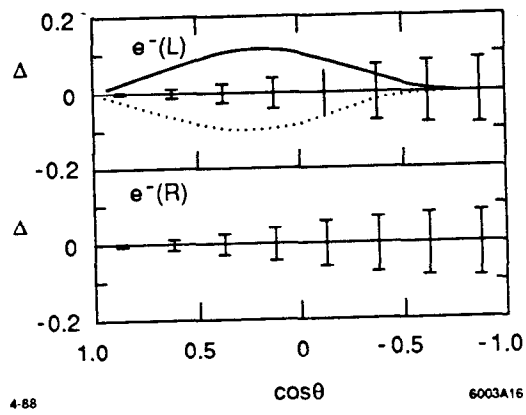


Figure 16. Contact interactions in Bhabha scattering, estimated as in Fig. 15 but using: $\Lambda = 30$ TeV, $\eta_{LL} = -1$, $\eta_{RR} = \eta_{RL} = 0$.

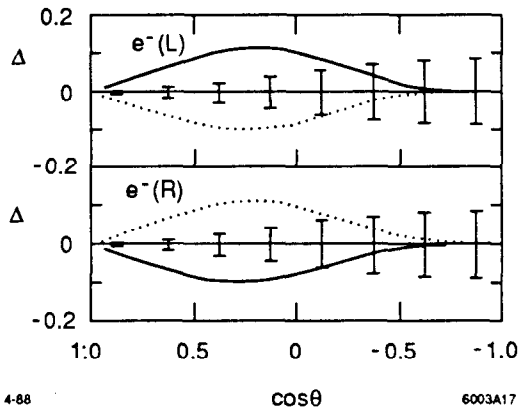


Figure 17. Contact interactions in Bhabha scattering, estimated as in Fig. 15 but using: $\Lambda = 30$ TeV, $\eta_{LL} = -\eta_{RR} = -1$, $\eta_{RL} = 0$.

the binding scale of leptons is near the TeV scale, we should expect to see extremely large cross section for e^+e^- reactions. Translating the geometrical estimate to R units, we have

$$\sigma \sim \frac{3}{4\pi\alpha^2} \frac{s}{\Lambda^2} R \sim 4500 \frac{s}{\Lambda^2} R. \quad (3.19)$$

Figure 18 shows the effect that one would see in the total cross section for $e^+e^- \rightarrow \mu^+\mu^-$ if the process can be mediated by a contact interaction with Λ in the few TeV range.^[6] If the compositeness of leptons is associated with the weak scale, its effects should be visible very soon; these effects might dominate the physics of TeV e^+e^- collisions.

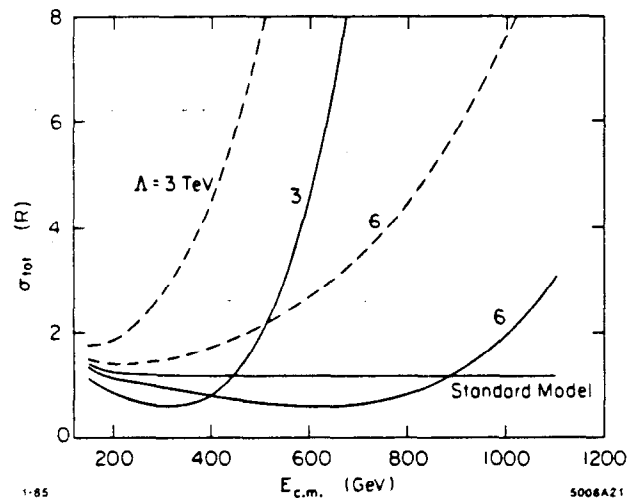


Figure 18. Effect of contact interactions on the total cross section for $e^+e^- \rightarrow \mu^+\mu^-$, for purely left-handed couplings (of either sign) and $\Lambda = 3$ 6 TeV.

4. New Z^0 Bosons

One effect which would be dramatically visible at a high-energy electron-positron collider is a new resonance, a new elementary vector boson coupling to e^+e^- annihilation. As we will see, such an object, if it exists, generates enormous cross sections, of order $10^4 R$ at the resonance peak. We should explore whether such an object is likely to appear and what its properties might be.

From a purely theoretical point of view, there is considerable motivation to expect further neutral weak bosons. Grand unified gauge theories began with the group $SU(5)$, the smallest group which envelops the $SU(3) \times SU(2) \times U(1)$ gauge

group of the standard model. But attempts to derive constraints on these theories and to solve problems of physics which arise in them led naturally to the consideration of larger grand unifying groups: $SO(10)$, E_6 , and others. The larger groups contain additional neutral bosons, and one can easily construct scenarios in which these bosons remain massless at the level of the grand symmetry breaking and so survive down to the weak scale. In particular, superstring models of unification naturally contain gauge bosons of an E_6 grand unifying group, and it is quite generic for extra neutral bosons to appear with masses below 1 TeV.^[34]

In principle, we might also expect charged bosons to appear, though the specific case of a right-handed W boson is ruled out below about 2 TeV through its potential influence on the K_L - K_S system.^[35] However, the constraints on new neutral bosons are surprisingly weak. Direct production experiments at hadron colliders are sensitive only a small distance beyond the familiar Z^0 .^[36] More stringent constraints come from the analysis of neutral-current weak interactions.^[37] One should also require that the mixing of the familiar Z^0 with the new boson not shift its mass by more than the 3 GeV tolerance permitted by the rapport between the standard model and experiment.^[38] These last two constraints on the mass and mixing angle of a new Z^0 are shown in Fig. 19.

The start of physics at the Tevatron Collider should significantly improve our knowledge of whether new neutral bosons exist. Neutral weak bosons are produced copiously at proton-antiproton colliders by quark-antiquark annihilation and are made visible in their decay to lepton pairs. If one assumes that 5 events of $p\bar{p} \rightarrow (e^+e^-) + X$, with all (e^+e^-) pairs in a single mass bin, would suffice to provide evidence of a new Z^0 , the curves in Fig. 20 show the potential of the Tevatron to discover a new Z^0 for two advertised levels of integrated luminosity. From the figure, it seems likely that, in the early 1990's, we will know if there is a new Z^0 boson with mass below 500 GeV. It seems quite appropriate, then, to anticipate the very interesting physics which would become accessible if such a state does appear.

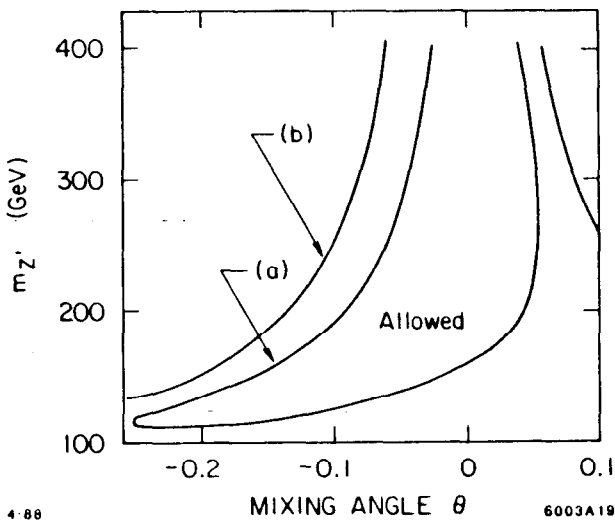


Figure 19. Constraints on the mass and mixing angle of a new neutral gauge boson (a) from the analysis of low-energy neutral current data (Ref. 37) and (b) from the constraint that the shift of m_Z be less than 3 GeV (Ref. 38). In both cases, couplings are assumed to be of the 'superstring-inspired' form (explained below).

4.1. EXTENDING THE STANDARD MODEL

The extended groups for grand unification, especially the exceptional group E_6 , strike fear into the hearts of experimentalists, but there is really nothing so difficult about them. In this section, I would like to describe enough of the group theory of extended models of grand unification to allow us to compute properties of new Z^0 bosons which arise from E_6 , including, in particular, the new bosons which appear in string-inspired theories. This can be done with very pedestrian means, requiring nothing more than a good understanding of $SU(3)$.^[39]

Why is E_6 interesting in the first place as a grand unifying group? The superstring theories have a special, and somewhat exotic, motivation for the appear-

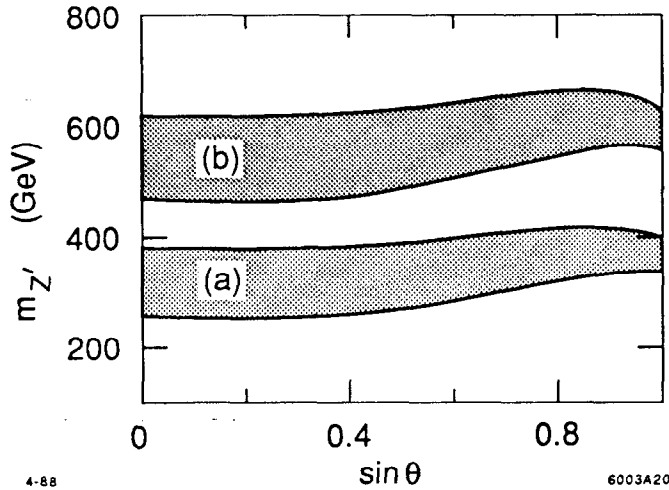


Figure 20. Mass values for a $Z'0$ boson corresponding to 5 events of $p\bar{p} \rightarrow Z'0 + X$; $Z'0 \rightarrow e^+ e^-$, at the Tevatron collider (a) for $\sqrt{s} = 1.8$ TeV, $\int \mathcal{L} = 10^{37}$, (b) for $\sqrt{s} = 2$ TeV, $\int \mathcal{L} = 10^{38}$. I take $K = 1.8$, consistent with CERN collider results, and structure functions from Ref. 10. The couplings of the $Z'0$, and the angle θ , are taken according to the scheme of Section 4.1. In this scheme, a generation of fermions contains exotic states in addition to the usual quarks and leptons; in each region, the upper bound assumes that these exotics are much heavier than the $Z'0$, and the lower bound assumes that they are much lighter.

ance of this group,^[40,41] but E_6 was originally introduced by Gürsey, Ramond, and Sikivie^[42] because it is a natural extension of $SU(5)$, bringing together the various components of the theory in a more symmetrical way.

The relation of E_6 to the components of $SU(5)$ is indicated in Fig. 21. The embedding of the standard model gauge group in $SU(5)$ is well-known. $SU(5)$ is the group of unitary transformations of a vector of 5 complex dimensions, and this sits naturally within the group $SO(10)$ of rotations of a 10-dimensional real vector. $SO(10)$ also contains the standard model gauge group in a different way, through the group $SU(3)_C \times U(1) \times SU(2)_L \times SU(2)_R$, where $SU(2)_L$ is the standard weak isospin, $SU(2)_R$ is its right-handed counterpart, the $U(1)$ is $(B-L)$, the difference of baryon and lepton number, and the $SU(3)_C$ is color. The embedding works because the groups $SU(2) \times SU(2)$ and $SU(4)$ happen to be identical to $SO(4)$

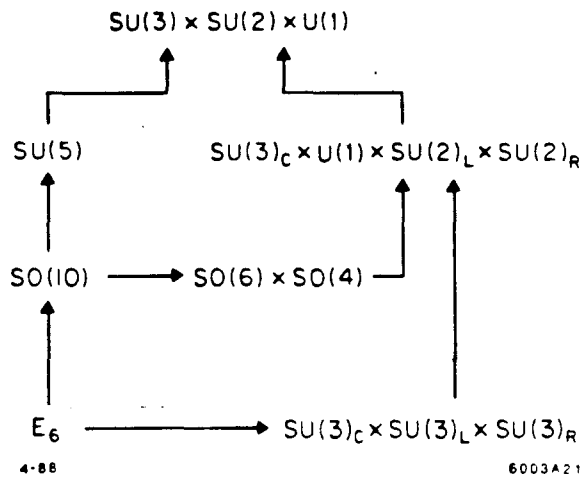


Figure 21. Embedding of the standard model gauge group in the exceptional group E_6 .

and $SO(6)$, respectively; $SU(3) \times U(1)$ is an obvious subgroup of $SU(4)$. This structure motivates the $SO(10)$ grand unified theory. One virtue of this theory is that the two separate fermion multiplets required for $SU(5)$ grand unification, the 5 and the $\overline{10}$, are unified into a single multiplet in $SO(10)$.

But now we can go one step further. The group $SU(3)_C \times U(1) \times SU(2)_L \times SU(2)_R$ can clearly be made more symmetrical by extending it to $SU(3)_C \times SU(3)_L \times SU(3)_R$. This group is the core of an extension of $SO(10)$ which gives precisely E_6 ; in fact, we can think of E_6 as the smallest simple group which contains this structure. The generators of E_6 which are relevant to phenomenology all live in this $SU(3) \times SU(3) \times SU(3)$ subgroup. Thus, we can understand the properties of extra neutral gauge bosons arising from E_6 by working with these $SU(3)$ components. Let me now reconstruct the properties of these bosons in the notation given by Langacker, Robinett, and Rosner.^[43]

$SU(3)$ has two diagonal generators, T^3 and hypercharge. Let me write these as

$$T^3 = \begin{pmatrix} \frac{1}{2} & & \\ & -\frac{1}{2} & \\ & & 0 \end{pmatrix}, \quad Y = \begin{pmatrix} 1 & & \\ & 1 & \\ & & -2 \end{pmatrix}. \quad (4.1)$$

The matrices T^3 and $(Y/\sqrt{12})$ form an orthonormal basis of generators, in the sense that

$$\text{tr}(T^3)^2 = \text{tr}\left(\frac{Y}{\sqrt{12}}\right)^2 = 0; \quad \text{tr}(T^3 \cdot Y) = 0. \quad (4.2)$$

Out of these ingredients, we can build an orthogonal set of commuting generators of E_6 . Clearly, we should begin by listing the standard model charges

$$T_C^3, \quad Y_C, \quad T_L^3. \quad (4.3)$$

The first two of these are the commuting generators of color, the third represents weak isospin. You can check that the more complex combination

$$\mathbf{Y} = T_R^3 - \frac{1}{6}(Y_L + Y_R) \quad (4.4)$$

is exactly the hypercharge Y of the standard model. There must be two more combinations of generators orthogonal to these. One is given by

$$\chi = 4T_R^3 + (Y_L + Y_R). \quad (4.5)$$

The combination of left and right hypercharges is just proportional to $(B-L)$, so χ lives inside $U(1) \times SU(2) \times SU(2)$, that is, inside $SO(10)$. The last orthogonal combination is

$$\psi = (Y_R - Y_L). \quad (4.6)$$

This last generator appears only when $SO(10)$ is extended to E_6 .

Now that we have explicit forms for the commuting charges of E_6 , we can work out the quantum numbers of fermions in any given E_6 representation. As is standard in grand unification, I consider all fundamental fermions to be left-handed; right-handed quarks are considered to be the antiparticles of left-handed antiquarks. To reconstruct a standard generation, we should study a multiplet of left-handed fermions in the fundamental representation, the **27**. This can be understood as the following symmetrical combination of representations of the three $SU(3)$ groups:

$$(\mathbf{3}, \overline{\mathbf{3}}, \mathbf{1}) + (\overline{\mathbf{3}}, \mathbf{1}, \mathbf{3}) + (\mathbf{1}, \mathbf{3}, \overline{\mathbf{3}}). \quad (4.7)$$

To understand the content of this representation in terms of standard models quantum numbers, we identify the quantum number under $SU(3)_C$ with color, decompose $SU(3)_L$ into weak isospin representations according to

$$\mathbf{3} \rightarrow \mathbf{2} + \mathbf{1}, \quad (4.8)$$

and break up the $\mathbf{3}_R$ into three $SU(2)_L$ singlets. The quantum numbers of the various fermions under the additional commuting generators may be computed from the explicit formulae (4.4) – (4.6). One should replace each T^3 or Y by 0 for a $\mathbf{1}$, by the appropriate diagonal element of (4.1) for a $\mathbf{3}$ and by the negative of this diagonal element for a $\overline{\mathbf{3}}$. For example, the component of the $(\mathbf{3}, \overline{\mathbf{3}}, \mathbf{1})$ which transforms as a $(\mathbf{3}, \mathbf{2})$ under color \times weak isospin has

$$\mathbf{Y} = -\frac{1}{6} \cdot (-1), \quad \chi = (-1), \quad \psi = -(-1). \quad (4.9)$$

Carrying out this evaluation for all of the fermions in the representation (4.7) gives the set of quantum numbers listed in Table 6. The particles denoted by a (*) comprise the members of a standard generation, plus the antiparticle of a right-handed neutrino. These states form an irreducible **16**-dimensional representation of $SO(10)$. The remaining particles, excluding the very last one, form a

Table 6: Quantum numbers of fermions in the **27** of E_6

	<u>Y</u>	<u>X</u>	<u>ψ</u>	<u>(ID)</u>	
$(\mathbf{3}, \bar{\mathbf{3}}, \mathbf{1}) \rightarrow (\mathbf{3}, \mathbf{2})$	1/6	-1	1	(u_L, d_L)	(*)
$(\mathbf{3}, \mathbf{1})$	-1/3	2	-2	D_L	
$(\bar{\mathbf{3}}, \mathbf{1}, \mathbf{3}) \rightarrow (\bar{\mathbf{3}}, \mathbf{1})$	1/3	3	1	(\bar{D}_R)	
$(\bar{\mathbf{3}}, \mathbf{1})$	-2/3	-1	1	(\bar{u}_R)	(*)
$(\bar{\mathbf{3}}, \mathbf{1})$	1/3	-2	-2	(\bar{d}_R)	(*)
$(\mathbf{1}, \mathbf{3}, \bar{\mathbf{3}}) \rightarrow (\mathbf{1}, \mathbf{2})$	-1/2	-2	-2	(N_L, E_L)	
$(\mathbf{1}, \mathbf{1})$	0	-5	1	$(\bar{\nu}_R)$	(*)
$(\mathbf{1}, \mathbf{2})$	1/2	2	-2	(\bar{N}_R, \bar{E}_R)	
$(\mathbf{1}, \mathbf{1})$	1	-1	1	(e_R^-)	(*)
$(\mathbf{1}, \mathbf{2})$	-1/2	3	1	(ν_L, e_L^-)	(*)
$(\mathbf{1}, \mathbf{1})$	0	0	4	S	

10-dimensional vector under $SO(10)$. The decomposition of the **27** into representations of smaller grand unifying group thus proceeds as indicated in Table 7. In general, the extension to E_6 brings in new fermions with exotic quantum numbers. These fermions may or may not be accessible at the new resonances, though they should have masses of order 1 TeV or below.

 Table 7: Decomposition of the **27** of E_6 into representations of $SO(10)$ and $SU(5)$

<u>E_6</u>	<u>$O(10)$</u>	<u>$SU(5)$</u>
	16	$10 + \bar{5} + 1$
27	\rightarrow +	\rightarrow +
	10	$5 + \bar{5}$
	+	+
	1	1

To turn this group-theory exercise into a set of definite predictions about physics, let me make the following assumptions about the spontaneous breaking of E_6 : First, I will assume that, in addition to the standard model gauge symmetry, one linear combination of χ and ψ remains unbroken at the scale of grand unification; the corresponding neutral vector boson $Z^{0'}$ should have a mass of order the

weak interaction scale. Second, I will assume that the ratio of the coupling of this new $U(1)$ boson to the coupling g' of the standard $U(1)$ factor in $SU(2) \times U(1)$ is not appreciably renormalized between the scale of grand unification and the weak scale. This assumption seems at first ad hoc, but Robinett and Rosner have shown that it holds in a wide class of models with a new Z^0 ^[44]. Finally, in accord with the conclusion of Fig. 19, I will ignore mixing of the $Z^{0'}$ with the familiar Z^0 .

To fix the extended neutral current Lagrangian, we should be careful to normalize the various $U(1)$ charges properly. Because the **27** contains 6 weak $SU(2)$ doublets, we have

$$\text{tr} (T_L^3)^2 = \frac{1}{2} \cdot 6 = 3. \quad (4.10)$$

Take this normalization as the standard. The sum of the squared hypercharges over the **27** can be assembled from Table 6; we find

$$\text{tr} (\mathbf{Y})^2 = 5. \quad (4.11)$$

Since, in the grand unified theory, the same coupling constant multiplies each generator with the same normalization, we have the following relation between the $SU(2)$ and $U(1)$ couplings:

$$g' = \sqrt{\frac{3}{5}} g. \quad (4.12)$$

This is the well-known statement that $SU(5)$ and its extensions predict $\sin^2 \theta_w = \frac{3}{8}$ at the scale of grand unification. Because the couplings g and g' obey different renormalization group equations, this relation is modified at lower energies and becomes $\sin^2 \theta_w \sim 0.22$ at the weak scale. We can continue this procedure to normalize χ and ψ ; from the table

$$\text{tr} (\chi)^2 = 120, \quad \text{tr} (\psi)^2 = 72. \quad (4.13)$$

This gives the relations

$$g_\chi = \frac{1}{2\sqrt{6}} g', \quad g_\psi = \frac{1}{6} \sqrt{\frac{5}{2}} g'. \quad (4.14)$$

Following Robinett and Rosner, we assume that these relations are not renormalized. To evaluate the coupling of the Z^0 at the weak scale, we thus use (4.14) directly with g' replaced by $(e/\cos\theta_w)$. Let us introduce an angle θ to parametrize which single linear combination of the normalized χ and ψ charges survives to the weak scale. Then the extended weak neutral current Lagrangian can be written

$$\begin{aligned}\mathcal{L}_{NC} = & e A_\mu J_{EM}^\mu + \frac{e}{\sin^2\theta_w \cos^2\theta_w} Z_\mu J_Z^\mu \\ & + \frac{e}{\cos^2\theta_w} Z'_\mu J_{Q'}^\mu,\end{aligned}\tag{4.15}$$

where the new charge Q' is given by

$$Q' = \left[\frac{1}{2\sqrt{6}} \sin\theta \cdot \chi - \frac{1}{6} \sqrt{\frac{5}{2}} \cdot \cos\theta \cdot \psi \right].\tag{4.16}$$

In the first superstring-inspired models containing only one extra $U(1)$ boson, a particular linear combination (4.16) was singled out.^[45] In these models, and more generally in models in which E_6 is broken by Higgs bosons in the adjoint representation, it is impossible to leave color and $SU(2)_L$ unbroken without also preserving Y_L . Then the unbroken $U(1)$ orthogonal to ordinary hypercharge will be a linear combination of \mathbf{Y} and Y_L . This can be arranged by setting $\sin\theta = \sqrt{3/8}$; then

$$Q' = \frac{1}{6}\eta, \quad \text{with} \quad \eta = \frac{3}{4}\chi - \frac{5}{4}\psi = 3\mathbf{Y} + \frac{7}{2}Y_L.\tag{4.17}$$

Whatever one might say about the logic of this choice, the ‘superstring inspired’ $U(1)$ boson does provide a particular, and quite generic, choice, in the middle of the phase space of the class of models I have defined.

4.2. PROPERTIES OF A Z^0' RESONANCE

Now that we have set up a concrete theory of a new Z^0 boson, we can straightforwardly work out its predictions for e^+e^- annihilation, on and off the new resonance. Even off of its dramatic resonance peak, the Z^0' creates substantial perturbations of the basic integral measures of fermion pair-production. To compute these effects, we simply return to the pair-production amplitudes given in eq. (2.5) and add the obvious additional term of the form

$$\frac{(Q')_e \cdot (Q')}{\cos^2 \theta_w} \frac{s}{s - m_{Z'}^2} . \quad (4.18)$$

For the right-handed components, $Q'(f_R) = -Q'(\bar{f}_L)$. Setting, as an example,

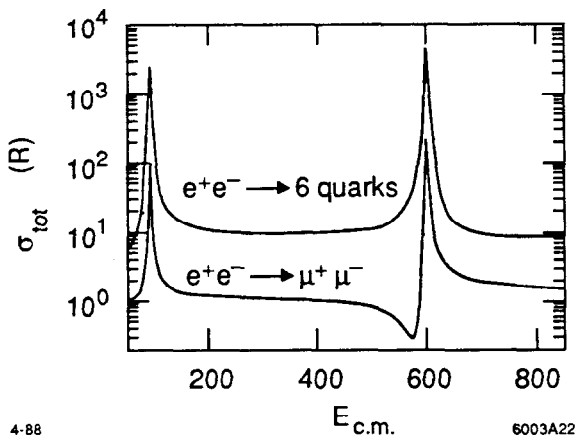


Figure 22. Total cross section for $e^+e^- \rightarrow \mu^+\mu^-$ and $e^+e^- \rightarrow q\bar{q}$, assuming six light quarks, including the effects of a new Z^0 boson.

$m_{Z'} = 600$ GeV and couplings of the ‘superstring-inspired’ form, we find the behavior of the total cross section, forward-backward asymmetry, and polarization asymmetry shown in Figs. 22–24. The presence of the new resonance is manifest

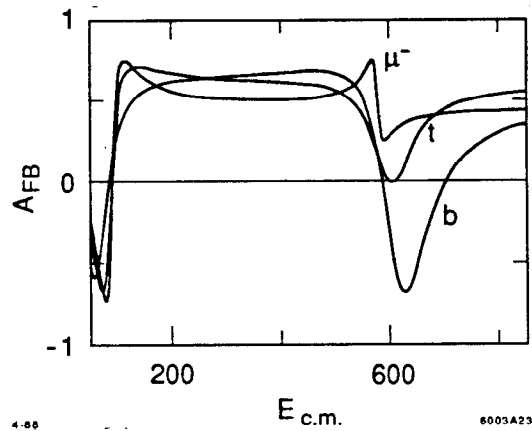


Figure 23. Forward-backward asymmetry for the production of μ , b and t pairs, including the effects of a new Z^0 boson.

in the whole region above the familiar Z^0 .

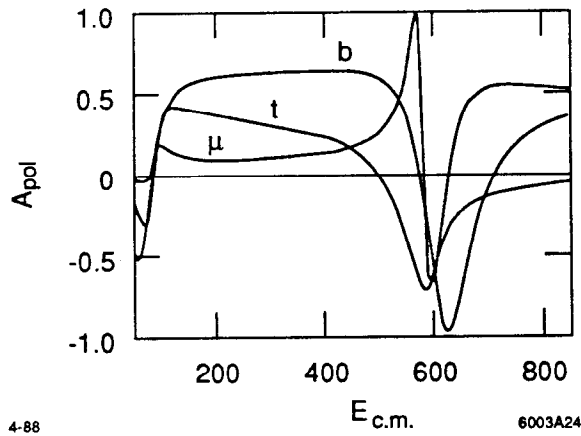


Figure 24. Polarization asymmetry for the production of μ , b , and t pairs, including the effects of a new Z^0 boson.

On resonance, the most important decays are to fermion pairs, and the relative importance of the various species reflects directly the particular linear combination of $U(1)$ currents to which the boson couples. The general expression for the decay

width to a particular mode is

$$\begin{aligned}
 \Gamma(Z^{0'} \rightarrow f\bar{f}) &= \frac{\alpha}{6 \cos^2 \theta_w} m_{Z'} \cdot (Q')^2 \\
 &= (0.78 \text{ GeV}) \cdot \left(\frac{m_{Z'}}{500 \text{ GeV}} \right) \cdot \left[\frac{\sin \theta}{2\sqrt{6}} \chi - \frac{\cos \theta}{6} \sqrt{\frac{5}{2}} \psi \right]^2. \quad (4.19)
 \end{aligned}$$

Table 8: Computation of the decay widths of a new gauge boson into quark and lepton pairs

	<u>L</u>	<u>R</u>	<u>total</u>	<u>fraction</u>
$\nu\bar{\nu}$	$\frac{1}{24}(3)^2$	x	$\frac{9}{24}$	16%
$\ell\bar{\ell}$	$\frac{1}{24}(3)^2$	$\frac{1}{24} \cdot 1^2$	$\frac{10}{24}$	18%
$u\bar{u}$	$\frac{1}{24}(-1)^2$	$\frac{1}{24} \cdot 1^2$	$\frac{2}{24}$	11%
$d\bar{d}$	$\frac{1}{24}(-1)^2$	$\frac{1}{24} \cdot (3)^3$	$\frac{10}{24}$	55%

The example of the pure $SO(10)$ gauge boson ($\sin \theta = 1$) is worked out in detail in Table 8, using the simplifying assumption that exotic states outside the standard generations are too heavy to be pair-produced. The various columns list the factors $(Q')^2$ for the left- and right-handed components of each fermion species, then convert these to relative branching fractions. Note the increased importance of the charged lepton decay mode relative to the familiar Z^0 , and the great importance of decays to $d\bar{d}$. Summing the weights and multiplying by 3 generations, we still arrive at a very small value for the width:

$$\Gamma_{\text{tot}} = 6.6 \text{ GeV}, \text{ for } m_{Z'} = 600 \text{ GeV} \quad (4.20)$$

and couplings, again, of the $SO(10)$ form. This calculation of the branching fractions has direct implications for the value of the peak cross section for production

of the $Z^{0'}$, through the formula

$$\sigma(e^+e^- \rightarrow Z^{0'}) = \frac{12\pi}{M_{Z'}^2} \frac{\Gamma(Z^{0'} \rightarrow e^+e^-)}{\Gamma_{\text{tot}}} = \frac{9}{\alpha^2} BR(Z^{0'} \rightarrow e^+e^-) R. \quad (4.21)$$

In the example worked out in Table 8, this gives the enormous value

$$\sigma_{\text{peak}} = 1010. R. \quad (4.22)$$

Such dramatic peaks appear quite characteristically in models with a new Z^0 boson below 1 TeV.

Given the presence of this huge resonance, the obvious experimental challenge is to determine the precise form of the current to which this new boson couples. One way to carry out this task would be to measure the asymmetries of fermion pair-production for various species. The forward-backward asymmetry just on resonance is given by

$$A_{FB} = 0.75 \frac{((Q'_{eL}Q'_{fL})^2 + (Q'_{eR}Q'_{fR})^2) - ((Q'_{eL}Q'_{fR})^2 + (Q'_{eR}Q'_{fL})^2)}{(Q'_{eL}Q'_{fL})^2 + (Q'_{eR}Q'_{fR})^2 + (Q'_{eL}Q'_{fR})^2 + (Q'_{eR}Q'_{fL})^2} \quad (4.23)$$

and the polarization asymmetry is given by

$$A_{\text{pol}} = \frac{(Q'_{eL})^2 - (Q'_{eR})^2}{(Q'_{eL})^2 + (Q'_{eR})^2}. \quad (4.24)$$

For production of lepton pairs, we have the relation

$$A_{FB} = 0.75(A_{\text{pol}})^2, \quad (4.25)$$

as on the familiar Z^0 . Cvetič, Lynn, and Stuart^[46] have noted that the three readily measured quantities

$$A_{\text{pol}}, \quad A_{FB}(e^+e^- \rightarrow t\bar{t}), \quad A_{FB}(e^+e^- \rightarrow b\bar{b}) \quad (4.26)$$

contain independent information and so may be used together as a powerful constraint on the $Z^{0'}$. Under the general assumptions I have given in Section 4.1, the t

quark always has a purely axial-vector coupling to the $Z^{0'}$, and so the asymmetry to $t\bar{t}$ vanishes. In Fig. 25, I plot the other two quantities from (4.26) against one another. It is clear from the plot that these two measurements, plus the test of the vanishing of the top quark asymmetry, determine the angle θ up to a twofold ambiguity and put the more general theoretical scheme to a severe test.

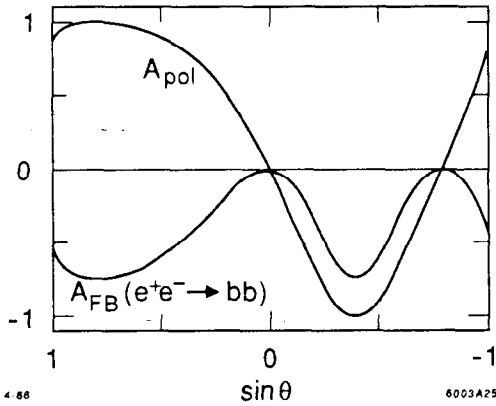


Figure 25. Comparison of the polarization asymmetry and the forward-backward asymmetry to $b\bar{b}$ on resonance for new Z^0 bosons of the class described in Section 4.1.

Throughout this section, I have ignored mixing of the $Z^{0'}$ with the familiar Z^0 . However, even a small mixing induces additional interesting effects. The most important of these is that the $Z^{0'}$ would now be allowed to decay to conventional weak bosons, opening up the following two processes

$$Z^{0'} \rightarrow W^+W^- , \quad Z^{0'} \rightarrow Z^0H^0 . \quad (4.27)$$

Figure 26 shows the peak cross sections for these processes for a 400 GeV $Z^{0'}$, as computed by Dib and Gilman.^[47] Apparently, the new resonance could be a source of insight not only into extensions of the standard model gauge group but also into the properties of the Higgs boson.

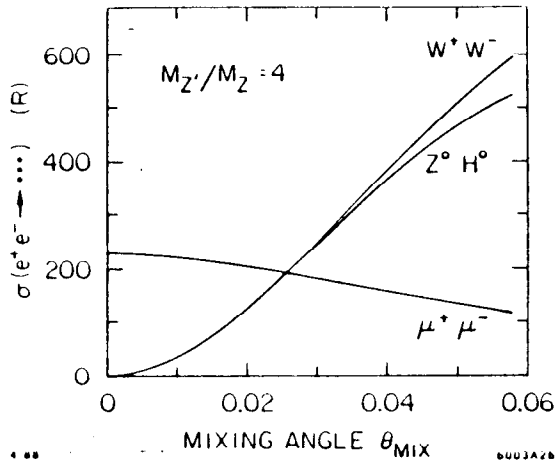


Figure 26. Peak cross sections for $e^+e^- \rightarrow Z^0$, followed by decay to W^+W^- and H^0Z^0 final states (from Ref. 47).

5. Higgs Boson and W Boson Physics

My final topic will be the processes at high-energy e^+e^- colliders which involve the production of Higgs bosons and W bosons. Given the philosophical orientation which I set out at the beginning of these lectures, this topic is probably the most crucial of all, since the reactions we will now discuss probe directly the nature of the mechanism of $SU(2) \times U(1)$ symmetry breaking. In addition, precisely because of their connection to symmetry breaking, the analysis of these processes brings in a new theoretical feature which I would like to discuss in some detail. The main theme of this section is that the production or scattering of massive vector bosons at high energy can be analyzed accurately in terms of the production of the corresponding Higgs particles; measurement of these cross sections measures the cross sections in the Higgs sector.

The idea of an identity between vector bosons and Higgs bosons comes directly from the Higgs mechanism of vector boson mass generation. In gauge theories, the vector bosons are required to be massless by the gauge symmetry principle. As massless vector particles, they have only two possible polarization states, the two transverse polarizations of a photon. If the symmetry is spontaneously broken,

the vector particles can obtain mass. In its own rest frame, the massive vector boson has spin 1 and hence must have 3 polarization states. Where did the extra degree of freedom come from? When a global symmetry is spontaneously broken, it is generally true (and I will show later in a concrete example) that the sector responsible for the symmetry-breaking must contain a massless scalar particle, called a ‘Goldstone boson’, with the quantum numbers of the symmetry current. If this current couples to a gauge boson, the Goldstone boson is absorbed into the gauge boson and mixes with it. This state provides the missing degree of freedom, and all 3 polarization states become massive.

This physical picture strongly suggests that the converse of the Higgs mechanism might also be true. At high energy, the transverse and longitudinal polarization states of a massive vector boson are cleanly distinguished. It is natural to suggest that the longitudinal polarization state has just the interactions of the Higgs scalar which was eaten up when the vector boson became massive. This Equivalence Theorem between longitudinal vector bosons and Higgs scalars was first introduced by Cornwall, Levin, and Tiktopoulos^[48] and Vayonakis^[49] and extended and clarified in a beautiful paper of Lee, Quigg, and Thacker.^[50] Recently, some very general proofs of the theorem have been presented by Chanowitz and Gaillard^[51] and Kunszt and Soper.^[52]

In this section, I will discuss this Equivalence Theorem and its ramifications for W boson and Higgs boson reactions at high energy. I will begin by presenting a formal argument for the theorem, and then working through a few relatively simple examples of its application. This will prepare us for a detailed analysis of the process $e^+e^- \rightarrow W^+W^-$; I will explain how this process provides a sensitive test of the gauge-theory structure of the weak interactions. I will then discuss reactions involving W boson scattering and Higgs boson production in W boson fusion. My discussion will draw heavily on the physical arguments presented in the papers of Lee, Quigg, and Thacker and Chanowitz and Gaillard cited above.

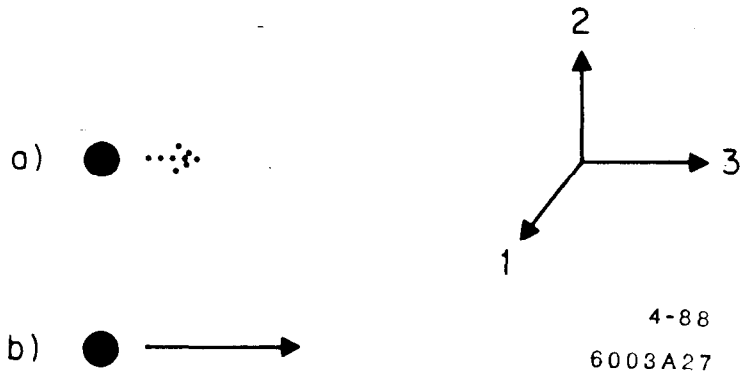


Figure 27. A massive vector boson (a) at rest and (b) in motion.

5.1. LONGITUDINAL W BOSONS, AND THE EQUIVALENCE THEOREM

I must begin with some formal discussion of the properties of longitudinal vector bosons in gauge theories. Consider a massive vector boson, first in its rest frame, and then in motion along the $\hat{3}$ axis (Fig. 27). In the rest frame, the vector particle may be polarized along the $\hat{1}$, $\hat{2}$, or $\hat{3}$ axes. Anticipating the boost, I will write the polarization vectors as

$$\begin{aligned}\epsilon_T^\mu(k) &= (0, \epsilon^1, \epsilon^2, 0) \\ \epsilon_L^\mu(k) &= (0, 0, 0, 1).\end{aligned}\tag{5.1}$$

The polarization vectors for the moving boson can be found by boosting (5.1) along the $\hat{3}$ axis:

$$\begin{aligned}\epsilon_T^\mu(k) &= (0, \epsilon^1, \epsilon^2, 0) \\ \epsilon_L^\mu(k) &= \left(\frac{k}{m}, 0, 0, \frac{E}{m}\right).\end{aligned}\tag{5.2}$$

A more invariant description of the same formulae is the following: for given vector boson momentum k^μ , the polarization vectors $\epsilon^\mu(k)$ are the three vectors satisfying $\epsilon^2 = -1$, $\epsilon \cdot k = 0$. The invariant sum over polarization vectors takes the form

$$\sum_\epsilon \epsilon^\mu(k) \epsilon^{\nu*}(k) = (-1) \cdot \left(g^{\mu\nu} - \frac{k^\mu k^\nu}{m^2} \right).\tag{5.3}$$

Both (5.2) and (5.3) make clear that there is something pathological about the lon-

itudinal polarization state: As $E \rightarrow \infty$, the components of ϵ_L^μ become extremely large, according to

$$\epsilon_L^\mu = \frac{k^\mu}{m} + \mathcal{O}\left(\frac{m}{E}\right). \quad (5.4)$$

Noting that ϵ_L^μ can become large without violating the conditions given above (5.3) because $k^2 = m^2$, so the square of the large term stays bounded. The vector ϵ_L^μ becomes large by becoming parallel to the large but increasingly lightlike vector k^μ .

How does this strangely singular polarization state arise from spontaneous symmetry breaking? Let me discuss this in the minimal version of the standard model, with one scalar doublet of Higgs particles. For simplicity, I will also ignore the $U(1)$ boson in the remainder of this section; that is, I will set $\sin^2 \theta_w = 0$.

The Lagrangian for the Higgs scalar doublet in the standard model takes the detailed form

$$\mathcal{L} = (D_\mu \varphi)^\dagger (D^\mu \varphi) - V(\varphi), \quad (5.5)$$

where

$$\varphi = \frac{1}{\sqrt{2}} \begin{pmatrix} \phi' + i\phi^2 \\ \phi^0 + i\phi^3 \end{pmatrix}, \quad D_\mu \varphi = (\partial_\mu - ig A_\mu^a \tau^a) \varphi \quad (5.6)$$

and $V(\varphi)$ is a potential energy for the φ field which favors spontaneous symmetry breaking. Expanding (5.5) in terms of the components of φ , we find

$$\mathcal{L} = \frac{1}{2} [(\partial_\mu \phi^0)^2 + (\partial_\mu \phi^a)^2] - V(\varphi) + g A_\mu^a J_\mu^a + \dots \quad (5.7)$$

where

$$J_\mu^a = i [\varphi^\dagger \tau^a \partial_\mu \varphi - \partial_\mu \varphi^\dagger \tau^a \varphi]. \quad (5.8)$$

Let us choose the following concrete form for $V(\varphi)$:

$$V(\varphi) = -\mu^2 (\varphi^\dagger \varphi) + \frac{\lambda}{2} (\varphi^\dagger \varphi)^2. \quad (5.9)$$

The point $\varphi = 0$ is unstable, and the minimum of V occurs at a value

$$\langle \varphi \rangle = \frac{1}{\sqrt{2}} \begin{pmatrix} 0 \\ \langle \Phi \rangle \end{pmatrix}, \quad \langle \Phi \rangle = \sqrt{2} \frac{\mu}{\sqrt{\lambda}}. \quad (5.10)$$

The curvature at the minimum of the potential gives the mass of the scalar boson in terms of the parameters of (5.9) as

$$m_H = \sqrt{2}\mu = \sqrt{\lambda} \langle \Phi \rangle. \quad (5.11)$$

The Lagrangian expanded around the minimum of the potential also contains a mass term for the vector field

$$\delta\mathcal{L} = g^2 \langle \varphi \rangle^\dagger (A_\mu \cdot \tau) (A_\mu \cdot \tau) \langle \varphi \rangle = \frac{1}{2} \left(\frac{g}{2} \langle \Phi \rangle \right)^2 A_\mu^a A_\mu^a. \quad (5.12)$$

In the simplest presentation of the theory, one can use the gauge symmetry to remove the fields ϕ^1, ϕ^2, ϕ^3 appearing in (5.6). However, it is interesting to calculate a bit further in a gauge such as the Feynman gauge which keeps these states present in the formalism. Expanding the potential $V(\varphi)$, one finds that they are massless; these are, indeed the Goldstone bosons associated with the spontaneous breaking of weak $SU(2)$. Expanding the current (5.8), one finds a term linear in the ϕ^a

$$J_\mu^a = \frac{1}{2} \langle \Phi \rangle \partial_\mu \phi^a + \dots \quad (5.13)$$

thus, the Lagrangian (5.7) contains a term which mixes the vector fields A_μ^a with the massless bosons. Long ago, Schwinger^[53] argued that this vertex is necessary to allow gauge bosons to become massive consistently with the fundamental equation of current conservation. We must insist that the gauge boson vacuum polarization

(Fig. 28(a)) satisfies $k_\mu \Pi^{\mu\nu} = 0$. But in order for this diagram to provide a

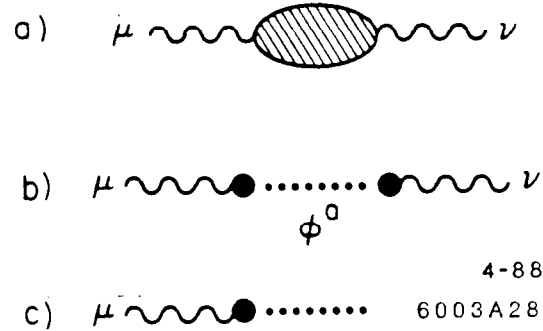


Figure 28. Vector boson vacuum polarization: (a) the basic form of the amplitude, (b) the pole term which allows mass generation, (c) the A^μ - ϕ mixing vertex.

mass for the vector boson, we must have $\Pi^{\mu\nu}(k) \rightarrow g^{\mu\nu}m^2$ as $k \rightarrow 0$. These two requirements are consistent with one another only if

$$\Pi^{\mu\nu}(k) \xrightarrow{k \rightarrow 0} \left(g^{\mu\nu} - \frac{k^\mu k^\nu}{k^2} \right) m^2. \quad (5.14)$$

But the $1/k^2$ singularity in the second term of this structure looks quite unusual. However, the A_μ - ϕ mixing vertex leads to the diagram of Fig. 28(b) whose value is

$$\left(ig \frac{\langle \Phi \rangle}{2} k^\mu \right) \frac{i}{k^2} \left(ig \frac{\langle \Phi \rangle}{1} k^\nu \right) = -i \left(\frac{g}{2} \langle \Phi \rangle \right)^2 \frac{k^\mu k^\nu}{k^2}. \quad (5.15)$$

This is of just the right form. We may identify the amplitude for A_μ - ϕ mixing to be

$$\text{Fig. 28} = i m k^\mu, \quad (5.16)$$

where m is the vector boson mass acquired through the Higgs mechanism.

This argument has a profound generalization to the couplings of a massive gauge boson. Following the logic of the previous paragraph, we recognize that the

boson vertex shown in Fig. 29(a) has two components: in the first, the boson couples directly to an internal line of the diagram, in the second, the boson mixes with the Goldstone boson, which in turn couples to the internal states. The Ward

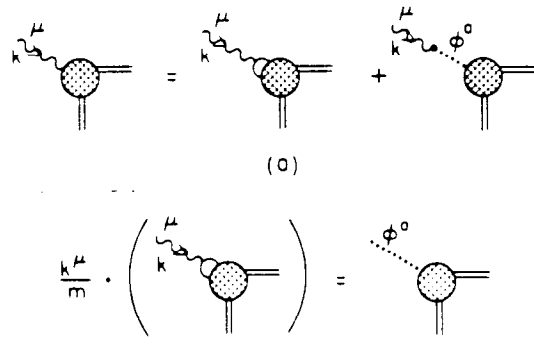


Figure 29. Vertex for emission of a massive gauge boson: (a) decomposition of the vertex into direct and indirect couplings; (b) effect of contracting the vertex with (k^μ/m) .

identity states that dotting k^μ into the vertex gives zero. We can simplify the contraction of k^μ with the second component of the vertex using the explicit form (5.16) of the mixing vertex

$$k^\mu \cdot \left(i m k^\mu \cdot \frac{i}{k^2} \right) = -m ; \quad (5.17)$$

this gives the diagrammatic identity shown in Fig. 29(b). Now, if the boson momentum k^μ is not collinear with any of the other external lines of the vertex, it will be a good approximation to replace (k^μ/m) by the longitudinal polarization vector $\epsilon_L^\mu(k)$. (This is not a good approximation for the dot product of k with the second component of the vertex shown in Fig. 29(a), but that hardly matters now.) The identity in Fig. 29(b) is then seen to be a relation which equates the coupling of a high-energy longitudinally polarized massive gauge boson with the coupling of the Goldstone scalar boson it ate up to become massive. This is the Equivalence

Theorem. It is presented diagrammatically in Fig. 30. (More complete proofs of the theorem, applicable to the case in which several longitudinal bosons couple to the same basic amplitude, are presented in Refs. 51 and 52.)

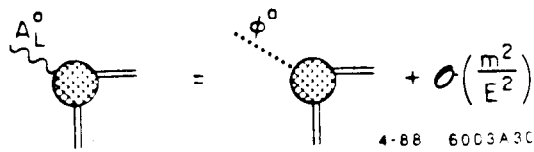


Figure 30. Statement of the Equivalence Theorem.

5.2. EXAMPLES OF THE EQUIVALENCE THEOREM

To clarify the physical content of the Equivalence Theorem, I would like to give a detailed analysis of three processes which provide simple illustrations of the result. All three of these processes are important in their own right as parts of the physics of Higgs and W bosons at high energy.

Let me first return to a formula which I presented, without extensive discussion, in Section 3.1. Look back at eq. (3.1), which gives the width for a heavy quark to decay to a light quark and an on-shell W boson. One might expect this width to be of order αM , where M is the heavy quark mass, but in fact it is enhanced by a further factor of $(M/m_W)^2$. To understand the origin of the enhancement, let us compute this decay rate explicitly. The vertex for W emission by a heavy quark (Fig. 31(a)) is

$$\mathcal{M} = \frac{g}{\sqrt{2}} \bar{u}(q) \gamma^\mu \left(\frac{1 - \gamma^5}{2} \right) u(Q) \epsilon_\mu^*(k) . \quad (5.18)$$

For simplicity, I will ignore the mass of the emitted quark. The square of this

amplitude, summed over final-state polarizations, is

$$\begin{aligned} \frac{1}{2} \sum_{\text{pol}} |\mathcal{M}|^2 &= \frac{g^2}{2} \frac{1}{2} \text{tr} \left\{ q \gamma^\mu \left(\frac{1 - \gamma^5}{2} \right) (Q + M) \gamma^\nu \left(\frac{1 - \gamma^5}{2} \right) \right\} \sum_{\text{pol}} \epsilon_\mu^*(k) \epsilon_\nu^*(k) \\ &= \frac{g^2}{2} [q^\mu Q^\nu + q^\nu Q^\mu - g^{\mu\nu} q \cdot Q] \cdot (-1) \left(g^{\mu\nu} - \frac{k^\mu k^\nu}{m_W^2} \right) . \end{aligned} \quad (5.19)$$

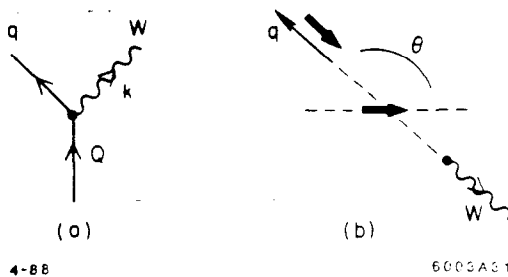


Figure 31. Decay of a massive quark to a light quark and a W boson: (a) decay vertex, (b) kinematics.

In the second line, I have summed over W polarizations using the formula (5.3). If the W is at high energy, the second term of the polarization sum gives the largest contribution, and (5.19) is well approximated by

$$\frac{1}{2} \sum_{\text{pol}} |\mathcal{M}|^2 \sim \frac{g^2}{2} \cdot 2 \frac{k \cdot q k \cdot Q}{m_W^2} . \quad (5.20)$$

For $M \gg m_W$, the final quark and the W each have energy approximately $(M/2)$, and (5.20) becomes just

$$\frac{1}{2} \sum_{\text{pol}} |\mathcal{M}| \sim \frac{2}{(\langle \Phi \rangle)^2} \frac{M^4}{2} . \quad (5.21)$$

We then recover

$$\Gamma = \frac{\alpha}{16 \sin^2 \theta_w} \frac{M^3}{m_W^2} . \quad (5.22)$$

If, instead of considering W emission by a heavy quark, we had considered Higgs boson emission, we would have been led to the same formulae. The vertex for a heavy quark to decay by emission of the Goldstone scalar is

$$\mathcal{M} = \lambda_f \bar{u}(q) \left(\frac{1 - \gamma^5}{2} \right) u(Q) . \quad (5.23)$$

Squaring, and inserting for the fermion-Higgs coupling λ_f the formula (1.6), we find

$$\frac{1}{2} \sum_{\text{pol}} |\mathcal{M}|^2 \sim \lambda_f^2 (Q \cdot q) , \quad (5.24)$$

which agrees exactly with (5.21). A byproduct of this analysis is an understanding of the angular dependence of W emission by a heavy quark. The kinematics is shown in Fig. 31(b). Since the W bosons mimic scalars, they carry off no spin. Since the final quark q must be left-handed, angular momentum dictates its angular distribution relative to the spin direction of the Q :

$$\frac{d\Gamma}{d\Omega} \sim 2 \sin^2 \frac{\theta}{2} \sim (1 - \cos \theta) . \quad (5.25)$$

The second process we will consider is the decay of a Higgs to W and Z boson pairs. For a standard neutral Higgs boson heavy enough that this decay is allowed, it is in fact the dominant mode. The reason for its large size should soon be clear.

To work out the decay vertex directly, we begin from the term of the standard model Lagrangian

$$\delta\mathcal{L} = \varphi^\dagger (g A_\mu \cdot \tau)^2 \varphi , \quad (5.26)$$

insert the component form (5.6), and shift ϕ^0 by its vacuum value (5.10). This

gives the vertices shown in Fig. 32. We can then compute

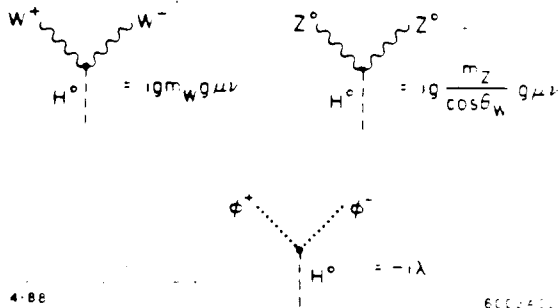


Figure 32. Feynman rules for Higgs coupling to boson pairs.

$$\begin{aligned} \Gamma(H \rightarrow W^+W^-) &= \frac{1}{2m_H} \cdot \frac{1}{8\pi} \cdot \left(1 - \frac{4m_W^2}{m_H^2}\right)^{\frac{1}{2}} \cdot (gm_W)^2 \\ &\cdot g^{\mu\nu} \left(g^{\mu\lambda} - \frac{k_+^\mu k_+^\lambda}{m_W^2}\right) \left(g^{\nu\sigma} - \frac{k_-^\nu k_-^\sigma}{m_W^2}\right) \cdot g^{\lambda\sigma} \end{aligned} \quad (5.27)$$

The two final factors arise from the sum over polarization states for the two W bosons. In each case, the largest contributions come from the $(k^\mu k^\lambda / m_W^2)$ terms. These terms yield the leading behavior

$$\Gamma(H \rightarrow W^+W^-) \sim \frac{\alpha}{16 \sin^2 \theta_w} \left(\frac{m_H^2}{m_W^2}\right) . \quad (5.28)$$

We can see the origin of the enhancement factor by dotting the approximate form of the longitudinal projector (k^μ / m_W) directly into the decay amplitude. This gives

$$\mathcal{M} \sim gm_W \cdot \frac{1}{2} \frac{m_H^2}{m_W^2} = \frac{g}{2} \frac{1}{\frac{1}{2}g \langle \Phi \rangle} \lambda \langle \Phi \rangle = \lambda , \quad (5.29)$$

where I have used (5.10) to introduce the Higgs scalar self-coupling λ . This amplitude for the Higgs to decay to a pair of longitudinal bosons agrees precisely with

the amplitude to decay to charged Goldstone scalars, which is also shown in Fig. 32.

Of course, the Equivalence Theorem gives only the leading behavior as m_H/m_W becomes large. From the direct calculation, on the other hand, we may obtain the complete expression for the decay width, including all powers of m_W/m_H . The result is

$$\begin{aligned}\Gamma(H \rightarrow W^+W^-) &= \frac{\alpha}{16 \sin^2 \theta_w} m_H \cdot \left(\frac{m_H}{m_W}\right)^2 \left(1 - 4 \frac{m_W^2}{m_H^2} + 12 \frac{m_W^2}{m_H^2}\right) \left(1 - \frac{4m_W^2}{m_H^2}\right)^{\frac{1}{2}}, \\ \Gamma(H \rightarrow Z^0Z^0) &= \frac{\alpha}{32 \sin^2 \theta_w} m_H \cdot \left(\frac{m_H}{m_Z}\right)^2 \left(1 - 4 \frac{m_Z^2}{m_H^2} + 12 \frac{m_Z^4}{m_H^4}\right) \left(1 - \frac{4m_Z^2}{m_H^2}\right)^{\frac{1}{2}}.\end{aligned}\quad (5.30)$$

The width of the Higgs due to its coupling to pairs of weak bosons is graphed in Fig. 33.

Finally, we turn to a first production mechanism for the Higgs boson, the reaction $e^+e^- \rightarrow H^0Z^0$. The process is clearly an important one, because it produces Higgs bosons tagged by their recoil against a Z^0 boson. It is therefore very interesting to work out the rate of this process and its angular distribution. The Feynman diagram contributing to the process is shown in Fig. 34(a). For future reference, I should remark that the fermionic part of this diagram has a very simple form; the current matrix element between states of definite helicity is

$$\bar{u}(p_+) \gamma^\mu \left(\frac{1 \pm \gamma^5}{2}\right) u(p) = \sqrt{s} \epsilon_\pm^\mu, \quad (5.31)$$

where, if $\hat{3}$ is the collision axis,

$$\epsilon_\pm^\mu = (0, \hat{1} \pm i\hat{2}). \quad (5.32)$$

With this information, we can write the amplitudes for production of H^0Z^0 from the two possible electron helicity states. For example, taking ϵ_-^μ and the appropriate Z^0 charge,

$$\mathcal{M}(e_L^- e_R^+ \rightarrow Z^0 H^0) = \sqrt{s} \epsilon_-^\mu \frac{e(\frac{1}{2} - \sin^2 \theta_w)}{\sin \theta_w \cos \theta_w} \cdot \frac{1}{s - m_Z^2} \cdot \frac{gm_Z}{\cos \theta_w} \cdot \epsilon_\mu^*(k) . \quad (5.33)$$

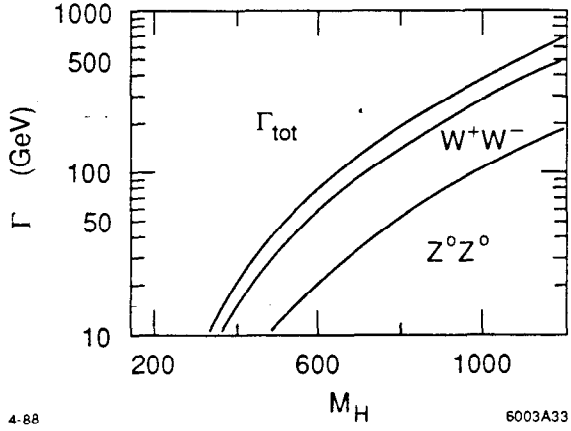


Figure 33. Expected total width of the single neutral scalar boson in the minimal version of the Higgs sector, and the contributions to this width from the most important sources: $H \rightarrow W^+W^-$ and $H \rightarrow Z^0Z^0$.

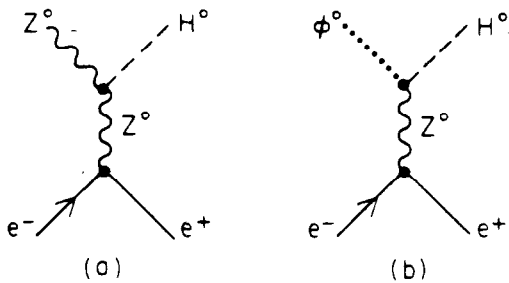
Once again, the largest contribution comes from the longitudinal polarization state of the vector boson, and we can account this by replacing $\epsilon_\mu^*(k)$ by (k^μ/m_Z) . Then

$$\mathcal{M}(e_L^- e_R^+ \rightarrow Z^0 H^0) \sim \sqrt{s} \epsilon_-^\mu \frac{e(\frac{1}{2} - \sin^2 \theta_w)}{\sin \theta_w \cos \theta_w} \cdot \frac{1}{s - m_Z^2} \cdot \frac{e}{\sin \theta_w \cos \theta_w} \cdot k_\mu . \quad (5.34)$$

This is exactly the amplitude for production of a Higgs boson pair—one scalar and one Goldstone—given by the diagram of Fig. 34(b).

The full expression for the differential cross section for $e^+e^- \rightarrow H^0 Z^0$ is^[50]

$$\frac{d\sigma}{d \cos \theta} = \frac{3}{64} \frac{(\frac{1}{2} - \sin^2 \theta_w)^2 + (\sin^2 \theta_w)^2}{2 \sin^4 \theta_w \cos^4 \theta_w} \cdot y \cdot \frac{y^2 \sin^2 \theta + 8m_Z^2/s}{(1 - m_Z^2/s)^2} , \quad (5.35)$$



4-86

6003A34

Figure 34. Description of the process $e^+e^- \rightarrow H^0Z^0$: (a) the Feynman diagram giving the transition amplitude, (b) a corresponding diagram related by the Equivalence Theorem.

where

$$y = \frac{2p}{\sqrt{s}} = \frac{[s^2 - 2s(m_H^2 + m_Z^2) + (m_H^2 - m_Z^2)^2]^{\frac{1}{2}}}{s} \quad (5.36)$$

In Fig. 35, I plot the differential cross section at 1 TeV for a variety of Higgs boson masses on the same coordinates that we used in Fig. 9 to exhibit the e^+e^- cross sections into vector boson pairs. Unfortunately, the Higgs cross sections are much smaller, no greater than 0.1 R in the mass range interesting for discovering the Higgs boson at a high-energy collider.

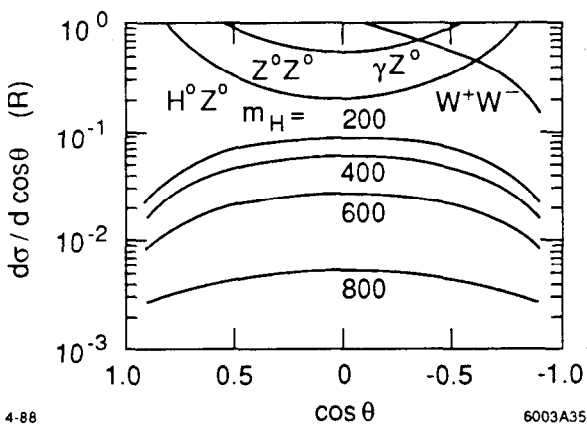


Figure 35. Differential cross sections for $e^+e^- \rightarrow H^0Z^0$, for various values of the Higgs boson mass, compared to the cross sections for vector boson pair-production.

5.3. THE REACTION $e^+e^- \rightarrow W^+W^-$

Having worked through a number of simple examples, we are ready to turn to two more involved applications of the Equivalence Theorem. The first of these is the process I described earlier as the largest single contribution to e^+e^- annihilation in the TeV region, the process of W boson pair-production. I will analyze this reaction in the following way: First, I would like to discuss in some detail the question of pair-production of longitudinally polarized W bosons. This polarization state is the most interesting from a physical point of view, and indeed we will see some unusual gauge-theory complications and a nontrivial application of the Equivalence Theorem. I will then present the cross sections to other polarization states and discuss the use of W pair-production as a test of the gauge structure of weak interactions.

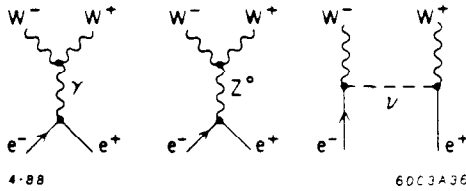


Figure 36. Feynman diagrams contributing to $e^+e^- \rightarrow W^+W^-$.

To leading order, the amplitude for W pair-production is given by the three Feynman diagrams of Fig. 36. Let us begin by analyzing the contribution of the first of these diagrams to production of a pair of longitudinally polarized W bosons. Since this diagram simply represents the electromagnetic production of charged bosons, we expect that its mathematical expression contains a term

$$\mathcal{M} \sim \sqrt{s} \epsilon_{\pm}^{\mu} \cdot \frac{e^2}{s} \cdot (k_+ - k_-)^{\mu} \epsilon^*(k_+) \cdot \epsilon^*(k_-) + \dots \quad (5.37)$$

Using the formula (3.6), we can see that this term alone contributes a cross section

(for each e^+e^- polarization state)

$$\frac{d\sigma}{d\cos\theta} = \frac{3}{8} \sin^2\theta |\epsilon(k_+) \cdot \epsilon(k_-)|^2 , \quad (5.38)$$

in units of R . Defining the $\hat{3}$ direction so that the final-state W bosons are travelling in opposite directions along this axis, we can write the longitudinal polarization vectors explicitly as

$$\epsilon_L(k_+) = \left(\frac{k}{m}, 0, 0, \frac{E}{m} \right) , \quad \epsilon_L(k_-) = \left(\frac{k}{m}, 0, 0, -\frac{E}{m} \right) . \quad (5.39)$$

Inserting (5.39) into (5.38), we find

$$\sigma_{\text{tot}} \sim \left(\frac{1}{4} R \right) \cdot \left(\frac{s}{m_W^2} \right)^2 . \quad (5.40)$$

This is a disaster! The cross section increases faster than permitted by unitarity by a factor of $(E_{\text{CM}}/m_W)^4$, and that due to the dynamics of only one partial wave.

If this problem is not somehow cured, it signals the breakdown of the simple gauge-theory description of weak interactions at energies above 1 TeV. In fact, the problem is cured within the gauge theory itself, by means of delicate cancellations among diagrams. These cancellations are simplest to work out for the initial state $e_R \bar{e}_L^\dagger$. In that case, the last diagram of Fig. 36 is absent and the first two diagrams are of exactly the same kinematic form, with relative coupling constants at

the various vertices as indicated in Fig. 37(a). The two diagrams cancel almost

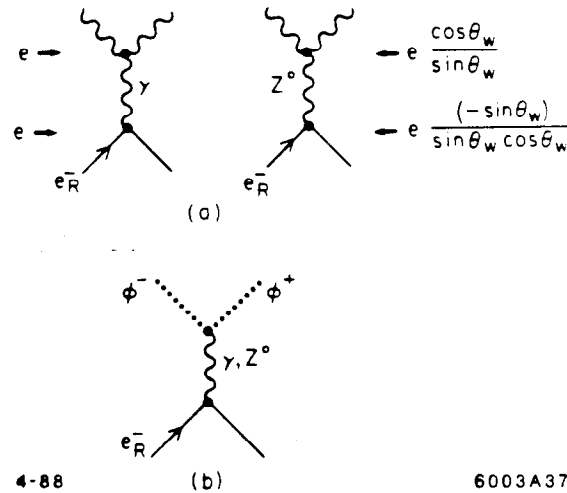


Figure 37. W pair-production from the initial state $e_R^- e_L^+$: (a) comparison of coupling constants in the two nonzero diagrams, (b) a second process related by the Equivalence Theorem.

completely; only terms involving the nonzero Z^0 boson mass remain. The sum of the two diagrams, for longitudinal final W bosons, takes the explicit form

$$\mathcal{M} = -ie^2\sqrt{s} \left(\frac{1}{s} - \frac{1}{s - m_Z^2} \right) \left(2\vec{\epsilon}_+ \cdot \vec{k}_+ \right) \left(\frac{2E^2 + m_W^2}{m_W^2} \right). \quad (5.41)$$

At very high energy, this is approximately equal to

$$\mathcal{M} \sim -ie^2\sqrt{s} \frac{1}{s} \left(2\vec{\epsilon}_+ \cdot \vec{k}_+ \right) \left(\frac{1}{2} \frac{m_Z^2}{m_W^2} \right). \quad (5.42)$$

This looks like the amplitude for electromagnetic and weak production of a pair of charged scalars. Indeed, by the Equivalence Theorem, we would expect this amplitude to be given at high energy by that for the process of Fig. 37(b), the

pair-production of Goldstone scalars. The photon and Z^0 exchange contributions to this latter process sum to

$$\mathcal{M} = \frac{-ie^2\sqrt{s}}{s} (2\vec{\epsilon}_+ \cdot \vec{k}_+) \cdot \left[1 + \frac{(-\sin^2 \theta_w)(\frac{1}{2} - \sin^2 \theta_w)}{\sin^2 \theta_w \cos^2 \theta_w} \right]. \quad (5.43)$$

If we note that the expression in the brackets reduces to simply $(1/2 \cos^2 \theta_w)$, we can see that this indeed agrees precisely with (5.42).

For the initial state $e_L^- e_R^+$, there are two further complications. First, the coupling of the electron-positron state to the Z^0 is changed to

$$e \frac{(\frac{1}{2} - \sin^2 \theta_w)}{\sin^2 \theta_w \cos^2 \theta_w} \quad (5.44)$$

so that the two diagrams in Fig. 37 no longer cancel. Second, there is an additional contribution from the diagram in which a neutrino is exchanged in the t -channel. To find the value of this diagram asymptotically for longitudinal final-state W bosons, let us replace the W polarization vectors by (k^μ/m_W) . Then the value of the third diagram in Fig. 36 becomes

$$\begin{aligned} \mathcal{M}^{\mu\nu} \cdot \frac{k_+^\mu}{m_W} \frac{k_-^\nu}{m_W} &= \frac{-ig^2}{2} \bar{v}_L \frac{\not{k}_+}{m_W} \frac{(\not{p}_- - \not{k}_-)}{(p_- - k_-)^2} \frac{\not{k}_-}{m_W} u_L \\ &= \frac{+ig^2}{2m_W^2} \bar{v}_L \not{k}_+ \frac{(\not{p}_- - \not{k}_-)(\not{p}_- - \not{k}_-)}{(p_- - k_-)^2} u_L \\ &= \frac{ig^2}{2m_W^2} \bar{v}_L \not{k}_+ u_L = \frac{-ie^2\sqrt{s}}{s} (2\vec{\epsilon}_- \cdot \vec{k}) \cdot \left(\frac{s}{m_W^2} \right). \end{aligned} \quad (5.45)$$

Adding together the contributions of the three diagrams, we find

$$M_{LL} = \frac{-ie^2\sqrt{s}}{s} (2\vec{\epsilon}_- \cdot \vec{k}) \cdot \left(\frac{m_W^2}{4 \sin^2 \theta_w m_W^2} \right). \quad (5.46)$$

This is just equal to

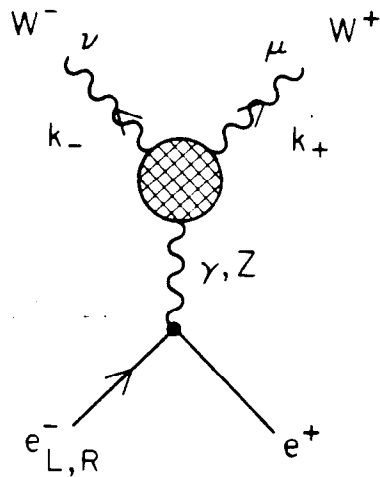
$$\frac{-ie^2\sqrt{s}}{s} (2\vec{\epsilon}_- \cdot \vec{k}) \left(1 + \frac{(\frac{1}{2} - \sin^2 \theta_w)^2}{\sin^2 \theta_w \cos^2 \theta_w} \right) \quad (5.47)$$

the contribution of the diagram of Fig. 37(b) for the initial state $e_L^- e_R^+$.

The main practical result of this analysis is that, while one might at first expect the pair-production cross section for longitudinal W bosons to be enhanced over the cross sections for other polarization states, delicate cancellations implicit in the gauge theory reduce this cross section back to the level of order 1 in units of R . Thus, in the standard model, transverse and longitudinal W bosons are produced at comparable rates. In order to study W cross sections experimentally, we must then worry about all possible polarization states. This leads to a very complicated expression for the standard model cross section, and further complications if we allow for possible deviations from the standard model. Hagiwara, Peccei, Zeppenfeld, and Hikasa^[54] have shown that one can cut through a certain amount of this complication by defining form factors for the vertex coupling a pair of W bosons to the photon and the Z^0 , and then considering the measurement of the W pair cross section as a measurement of these form factors. Assuming CP conservation, the general form of the W - W -boson vertex can be parametrized by four form factors. Let us define these by writing the amplitude of Fig. 38 in the form

$$\begin{aligned} & ie^2\sqrt{s} \epsilon_{\pm}^{\lambda} \frac{1}{s} \epsilon_{\mu}(k_+) \epsilon_{\nu}(k_-) \\ & \cdot \left\{ g^{\mu\nu} (k_- - k_+)^{\lambda} F_1 - \frac{(k_- - k_+)^{\lambda} k_-^{\mu} k_+^{\nu}}{m_W^2} F_2 \right. \\ & \left. + (g^{\mu\lambda} k_+^{\nu} - g^{\nu\lambda} k_-^{\nu}) F_3 + i\epsilon^{\mu\nu\lambda\sigma} (k_- - k_+)_{\sigma} F_5 \right\} . \end{aligned} \quad (5.48)$$

(Note that this convention differs slightly from that of Ref. 54.) The amplitude



4-88

6003A38

Figure 38. Amplitude used in defining the W - W -photon and W - W - Z^0 form factors.

F_1 is the electric form factor; F_3 gives the magnetic moment of the W . In the standard model, at leading order,

$$F_1 = F_3 = \frac{1}{\sin^2 \theta_w} I^3 \frac{s}{s - m_W^2} + Q \left(1 - \frac{s}{s - m_Z^2} \right) \quad (5.49)$$

$$F_2 = F_5 = 0.$$

Here I^3 denotes weak isospin: $I^3 = -\frac{1}{2}$ for e_L^- and vanishes for e_R^- .

It is not difficult to work out explicit formulae, in terms of the form factors defined in (5.48), for the cross sections for production of each W polarization state from electron and positron initial states of definite helicity. The cross sections for production of a pair of transverse W bosons, a mixed pair, and a pair of longitudinal

W bosons are given, respectively, by

$$\begin{aligned}
 \left(\frac{d\sigma}{d\cos\theta} \right)_{TT} &= \frac{3}{8}\beta \cdot \left\{ 2|A_1|^2 \sin^2\theta - 4\text{Re}(A_1^*A_2) \cos\theta \sin^2\theta \right. \\
 &\quad \left. + 2|A_2|^2 \sin^2\theta (1 + 2\cos^2\theta) \right\} \\
 \left(\frac{d\sigma}{d\cos\theta} \right)_{TL+LT} &= \frac{3}{8}\beta \cdot \left\{ 2|A_3|^2 (1 + \cos^2\theta) + 4\text{Re}(A_3^*A_4) \cos\theta \sin^2\theta \right. \\
 &\quad \left. + 2|A_4|^2 \sin^4\theta \right\} \\
 \left(\frac{d\sigma}{d\cos\theta} \right)_{LL} &= \frac{3}{8}\beta \cdot \left\{ |A_5|^2 \sin^2\theta \right\} ,
 \end{aligned} \tag{5.50}$$

where $\beta = (1 - 4m_W^2/s)^{\frac{1}{2}}$ is the W velocity. For the $e_L^- e_R^+$ initial state, the amplitudes A_i are given by

$$\begin{aligned}
 A_1 &= \beta \left(F_1 + \frac{1}{2\sin^2\theta_w} \frac{1}{D} \right) \\
 A_2 &= \frac{1}{2\sin^2\theta_w} \frac{1}{D} \\
 A_3 &= \beta \frac{s}{\sqrt{m_W}} \left(\frac{1}{2} F_3 + \frac{1}{2\sin^2\theta_w} - \frac{1}{2} \beta \cos\theta F_5 \right) \\
 &\quad + \frac{1}{\sin^2\theta_w} \frac{m_W}{\sqrt{s}} \frac{1}{\beta} \left(1 - \frac{2m_W^2}{s} \frac{1}{D} \right) \\
 A_4 &= -\frac{1}{2} \beta^2 \frac{\sqrt{s}}{m_W} F_5 + \frac{1}{\sin^2\theta_w} \frac{m_W}{\sqrt{s}} \frac{1}{D} \\
 A_5 &= \beta \frac{s}{m_W^2} \left(\frac{1}{2} F_3 - \frac{1}{2} F_1 + \frac{1}{4\sin^2\theta_w} + \frac{\beta^2}{4} \frac{s}{m_W^2} F_2 \right) \\
 &\quad + \beta F_1 + \frac{1}{\beta \sin^2\theta_w} \left(1 - 2 \frac{m_W^2}{s} \frac{1}{D} \right) ,
 \end{aligned} \tag{5.51}$$

with

$$D = \frac{1}{2}(1 + \beta^2 - 2\beta \cos \theta). \quad (5.52)$$

The corresponding formulae for $e_R^- e_L^+$ are given by dropping all terms in (5.51) which do not explicitly involve the form factors F_i , changing the sign of the F_5 terms, and changing the F_i themselves to their new appropriate values (given, at leading order, by eq. (5.49) with $I^3 = 0$).

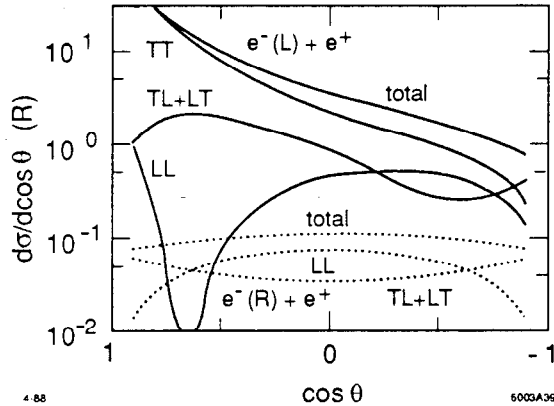


Figure 39. Cross section for $e^+e^- \rightarrow W^+W^-$ for polarized e^- and unpolarized e^+ beams, at $\sqrt{s} = 300$ GeV. For each e^- helicity, the decomposition of the total cross section into the various W polarization states is shown.

The numerical values of the leading-order cross sections, for two values of \sqrt{s} , are shown in Figs. 39 and 40. The solid and dotted curves show the dependence on e^- polarization; note that, even in the backward region where the s -channel diagrams contribute substantially, the cross section from e_R^- is always very small. For e_L^- , the cross section is dominated by a forward peak associated with the t -channel neutrino exchange diagram. The peak is made up entirely from production of transverse W pairs. We have argued already that, at high energy, the cross section for production of longitudinal W pairs takes on a $\sin^2 \theta$ angular distribution. In the backward hemisphere, this longitudinal W production accounts for about 25% of the total cross section.

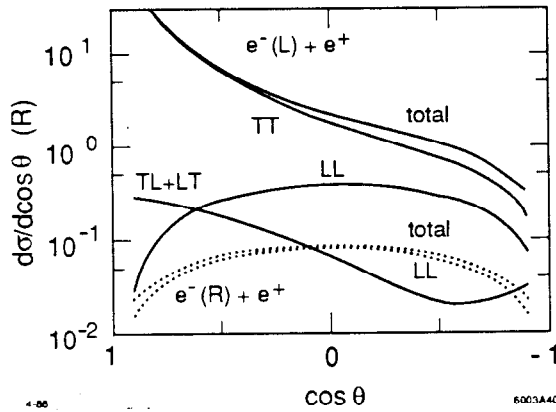


Figure 40. Cross section for $e^+e^- \rightarrow W^+W^-$ for polarized e^- and unpolarized e^+ beams, at $\sqrt{s} = 1$ TeV.

From the arguments given at the beginning of this section, it is easy to see that any disruption of the gauge theory structure of W boson couplings leads to large corrections to the standard model formulae. In the amplitude for production of a pair of longitudinal bosons, these corrections can be enhanced by a factor of (s/m_W^2) ; thus, they are readily visible. As a particular, simple example of this effect, let us work out the consequences of including a fundamental anomalous magnetic moment for the W . To avoid excessive complication, let me assume the same anomalous moment in the photon and Z^0 couplings, so that the cancellations in the e_R^- amplitude go through as before. Thus, I assume

$$F_1 = \frac{1}{\sin^2 \theta_w} I^3 \frac{s}{s - m_W^2} + Q \left(1 - \frac{s}{s - m_Z^2} \right) \quad (5.53)$$

$$F_3 = F_1 \cdot \left(1 + \frac{g-2}{2} \right).$$

The effect of this change is shown in Figs. 41 and 42. Figure 41 shows how the assumption of even a small $(g-2)$ changes both the normalization and the shape of the W pair-production cross section. The figure makes clear that the

changes arise from an enormous growth in the production of longitudinal W pairs.

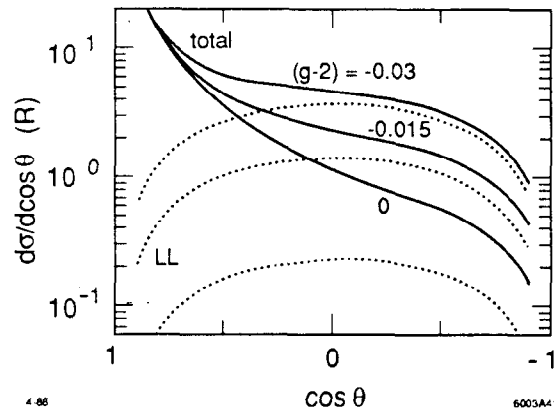


Figure 41. Effect on the cross section for $e^+e^- \rightarrow W^+W^-$ at $\sqrt{s} = 1$ TeV, using unpolarized electrons) of a fundamental anomalous magnetic moment for the W , introduced according to the scheme of eq. (5.53). The dotted curves show the contributions from the longitudinal W production alone.

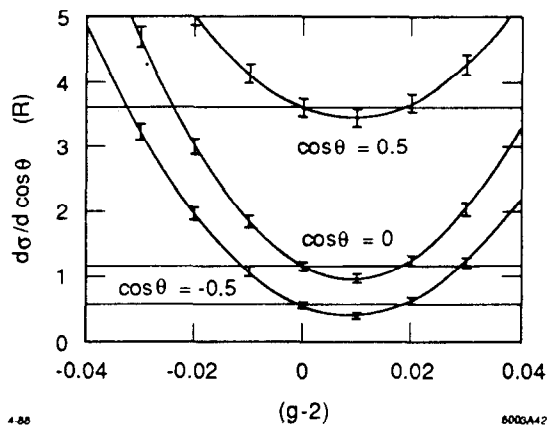


Figure 42. An experiment to measure the fundamental $(g-2)$ of the W boson: The curves show the theoretical predictions, following from (5.53), for the differential cross-section at three angles θ . The statistics reflect the events in an integrated luminosity of 3000 R^{-1} with one hadronic and one leptonic W boson decay, divided into four bins in $\cos \theta$.

Figure 42 converts this calculation into a (thought) experiment to measure $(g - 2)$, with statistics available at the 1 TeV collider envisioned in Section 1.2. A more subtle correction, which occurs even within the standard model, is the introduction of a new, very heavy fermion generation. Ahn, Lynn, Selipsky, and I^[55] have shown that, because the radiative corrections due to this heavy fermion appear asymmetrically between the s - and t -channel diagrams, one can find contributions from the radiative corrections which are enhanced by a factor (s/m_W^2) . This leads

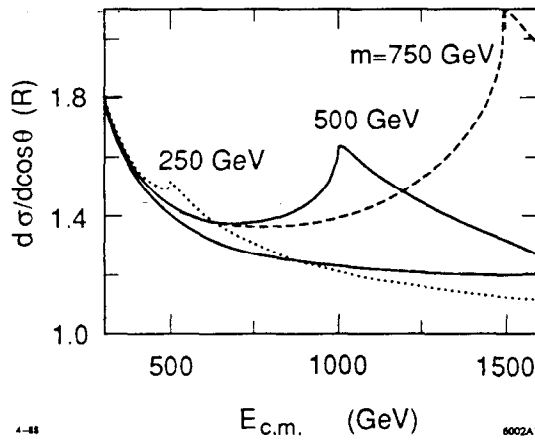


Figure 43. Effect of a new generation of heavy fermions on the cross section $d\sigma/d\cos\theta$ for W pair production at $\cos\theta = 0$, shown as a function of \sqrt{s} .

to the effect shown in Fig. 43, which should allow experiments at a high energy collider to obtain evidence for even those quark generations too heavy to be pair-produced.

5.4. HIGGS PRODUCTION BY W FUSION

Our second nontrivial example of the Equivalence Theorem occurs in processes involving internal W bosons radiated from the electron and positron. At center-of-mass energies much higher than m_W , we should expect the appearance of a W boson analogue of the two-photon process. In this process, shown diagrammatically

in Fig. 44(a), the electron and positron emit collinear virtual W bosons. The amplitude for W emission is largest when the W bosons are relatively close to mass shell, so the collision amplitude in the center of the diagram is a close approximation to the scattering amplitude of on-shell W bosons. At very high energy (this is still not quite accurate at 1 TeV), we can describe the virtual W bosons as partons of the electron and positron.^[56,57]

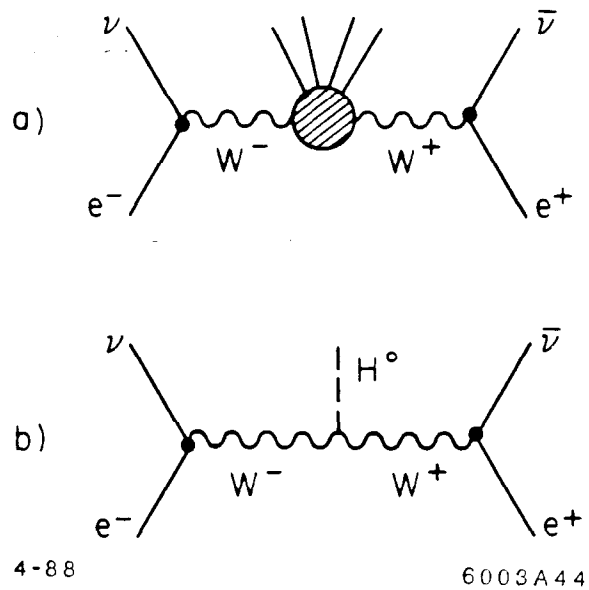


Figure 44. The W boson analogue of the two-photon process: (a) general structure of the process; (b) mechanism of Higgs boson production by W fusion.

An important example of this process is the reaction shown in Fig. 44, a process identified by Jones and Petcov^[58] and Cahn and Dawson^[59] as giving a large cross section for the production of a standard neutral Higgs boson. In this process, the amplitude which appears in the center of the diagram is the inverse of the Higgs decay amplitude to W bosons; we found above that this amplitude is dominated by the contribution from longitudinal W bosons. More generally, the Equivalence Theorem tells us that the contribution to the WW process from collisions of longitudinal W bosons is directly proportional to the

scattering amplitude of Higgs Goldstone scalars. Thus, we would very much like to be able to measure this longitudinal W contribution to the WW process. This contribution will be large if there is a large amplitude for the electron and positron to emit a longitudinal W .

At first sight, though, the probability of finding a longitudinal W seems very small. The Equivalence Theorem would seem to say that the coupling of a longitudinal W to the electron is proportional to the electron coupling to a Goldstone scalar, that is, to the electron-Higgs couplings constant

$$\lambda_e \sim \frac{m_e}{\langle \Phi \rangle} \sim 10^{-5}. \quad (5.54)$$

It is clear from this estimate that we cannot find cross sections of interesting size unless there are large corrections to the Equivalence Theorem in this particular circumstance. We can shed some important light on the theorem by explaining why, in fact, there are corrections which lead to substantial longitudinal W contributions. Our discussion will follow the analysis of Chanowitz and Gaillard.^[51]

Since we wish to explore the corrections to the Equivalence Theorem, we should begin by writing the leading correction to the approximation (5.4) to the longitudinal polarization vector. For $E \gg m_W$,

$$\epsilon_L(k) = \left(\frac{k}{m} 0, 0, \frac{E}{m} \right) \cong \frac{k^\mu}{m} - \frac{m}{2E^2} \tilde{k}^\mu, \quad (5.55)$$

where \tilde{k}^μ is the momentum of a W moving in the $(-\hat{3})$ direction

$$\tilde{k}^\mu = (E, 0, 0, -k). \quad (5.56)$$

Let us assume that we can apply this formula off-shell and use it to compute the

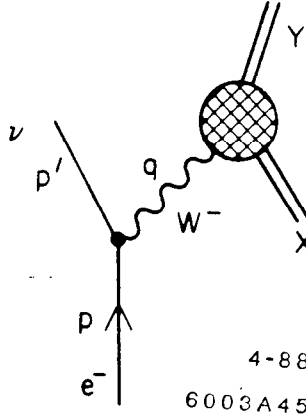


Figure 45. A process involving collinear emission of a virtual W .

contribution to the diagram of Fig. 45 from a longitudinal W close to mass shell. Let us label the initial electron momentum, the final neutrino momentum, and the W momentum q by writing

$$\begin{aligned} p &= E(1, 0, 0, 1) \\ p' &= (1-x)E(1, 0, 0, 1) + p_{\perp} \\ q &= xE(1, 0, 0, 1) - p_{\perp} . \end{aligned} \quad (5.57)$$

The parameter x is the longitudinal fraction of the W , viewed as a parton of the electron. Then the cross section for the process of Fig. 45 is

$$\begin{aligned} \int d\sigma(e_L^- X \rightarrow \nu Y) \\ \cong \frac{1}{2s} \int \frac{d^3 p'}{(2\pi)^3 2p'} \left| \frac{g}{\sqrt{2}} \bar{u}_L \gamma^\mu u_L \epsilon_L^\mu(q) \frac{1}{(p-p')^2 - m_W^2} \mathcal{M}(W_L X \rightarrow Y) \right|^2 . \end{aligned} \quad (5.58)$$

Rewriting (5.55) in terms of the momentum of the initial electron,

$$\epsilon_L^\mu(q) \cong x \frac{p^\mu}{m_W} - \frac{m_W^2}{2xE^2} \tilde{p}^\mu . \quad (5.59)$$

Since

$$\bar{u}(p') \not{p} u_L(p) = 0, \quad \bar{u}_L(p') \not{p} u_L(p) = \sqrt{s} \cdot \sqrt{s(1-x)}, \quad (5.60)$$

the cross section (5.58) takes the following form for a virtual longitudinal W :

$$\begin{aligned} & \int d\sigma(e_L^- X \rightarrow \nu Y) \\ & \sim \frac{1}{2s} \int_0^1 \frac{dx}{x} \frac{1}{16\pi^2} \frac{g^2}{2} \left(\frac{2m_W}{xs} \right)^2 s^2(1-x) \cdot \int d^2 p_2 \frac{1}{(p_{\perp}^2 + m_W^2)^2} |\mathcal{M}|^2. \end{aligned} \quad (5.61)$$

The next-to-last term in this equation is the W transverse momentum distribution; it is steeply peaked about zero, with a width $\Delta p_{\perp} \sim m_W$. Integrating over the peak, we find

$$\begin{aligned} & \int d\sigma(e_L^- X \rightarrow \nu Y) \\ & \sim \frac{1}{2s} \int \frac{dx}{x} \frac{g^2}{8\pi^2} m_W^2 \frac{1-x}{x^2} \cdot \left(\frac{\pi}{m_W^2} \right) |\mathcal{M}|^2 \\ & \sim \int_0^1 \frac{dx}{x} \left(\frac{\alpha}{2\pi \sin^2 \theta_w} \frac{1-x}{x} \right) \sigma(w_L(xp) X \rightarrow Y). \end{aligned} \quad (5.62)$$

Note that the integral over the transverse momentum distribution generates a factor of m_W^{-2} which cancels the factor m_W^2 from the correction term in (5.59). The final result is a smooth distribution function, independent of the W mass, for finding a longitudinal W in the electron:

$$f_{WL}(x)dx = \frac{dx}{x} \left(\frac{\alpha}{2\pi \sin^2 \theta_w} \frac{1-x}{x} \right). \quad (5.63)$$

This function is similar in its general character to the Weizsäcker-Williams distribution of photons generated by an electron, except that the enhancement factor $\log(s/m_e^2)$ does not appear. (The distribution function for transverse W bosons does have an enhancement factor $\log(s/m_W^2)$.)

How did we manage to get a substantial result for an amplitude forbidden by the Equivalence Theorem? Look back to the proof which I gave in Section 5.1, and you will see that I assumed that the W boson coupled to external states which were not collinear with its momentum. In other words, I assumed that the W was at high energy with respect to all other external particles. In this example, the vertex for W emission from the electron line could be boosted to a frame where the W is moving slowly and the electron and neutrino have relatively low energy. In this frame, the Equivalence Theorem has no reason to apply. The final result is just as we might have wished: The Equivalence Theorem can be used to analyze the WW scattering process in the center of Fig. 44, but it cannot be used to argue the suppression of longitudinal W couplings to the external electron and positron lines.

To understand the idea of W parton distributions more concretely, let us analyze explicitly the amplitude for the process of Fig. 44(b), $e^+e^- \rightarrow \nu\bar{\nu}H^0$. Letting p represent the initial electron momentum, p' the final neutrino momentum, q the W momentum, and \bar{p} , \bar{p}' , \bar{q} the corresponding quantities on the positron side, the Feynman diagram of Fig. 44(b) leads to the following expression for the total cross section:

$$\begin{aligned}
\sigma &= \frac{1}{2s} \int \frac{d^3 p'}{(2\pi)^2 2p'} \frac{d^3 \bar{p}'}{(2\pi)^2 2\beta'} \frac{d^3 p_H}{(2\pi)^2 - m_W^2} (2\pi)^4 \delta(\Sigma p) \\
&\quad \cdot \left| \left(\frac{g}{\sqrt{2}} \right)^2 \bar{u} \gamma^\mu u_L \frac{g^{\mu\nu}}{(p - p')^2 - m_W^2} (gm_W) \frac{g^{\nu\lambda}}{(\bar{p} - \bar{p}')^2 - m_W^2} \bar{u}_L \gamma^\lambda u_L \right|^2 \\
&\sim \frac{1}{2s} \int_0^1 \frac{dx}{x} \int \frac{d^2 p_\perp}{16\pi^3} \frac{g^2}{(p_\perp^2 + m_W^2)^2} \int \frac{d\bar{x}}{\bar{x}} \int \frac{d^2 \bar{p}_\perp}{16\pi^3} \frac{g^2}{(\bar{p}_\perp^2 + m_W^2)^2} \\
&\quad \cdot (2\pi) \delta(q + \bar{q})^2 - m_H^2 \cdot \frac{g^2 m_W^2}{4} \cdot [16 p \cdot \bar{p}' p' \cdot \bar{p}] . \tag{5.64}
\end{aligned}$$

The second line assumes that the momenta p' , \bar{p}' are both steeply peaked forward.

Integrating over the two peaks, we find

$$\begin{aligned}\sigma \sim & \frac{1}{2s} \int \frac{dx}{x} \int \frac{d\bar{x}}{\bar{x}} \left(\frac{\alpha}{4\pi^2 \sin^2 \theta_w} \right)^2 \\ & \cdot \left(\frac{\pi}{m_W^2} \right)^2 \frac{4\pi\alpha}{\sin^2 \theta_w} m_W^2 s^2 (1-x)(1-\bar{x}) \cdot 2\pi\delta(\hat{s} - m_H^2) .\end{aligned}\quad (5.65)$$

Compare this to the cross section for $W_L^+ W_L^- \rightarrow H^0$, which can be reconstructed from the formula (5.28) for the Higgs width to $W_L^+ W_L^-$:

$$\begin{aligned}\sigma(W_L^+ W_L^- \rightarrow H^0) &= \frac{16\pi^2}{m_H} \Gamma(H \rightarrow W^+ W^-) \delta(\hat{s} - m_H^2) \\ &= \frac{\pi^2 \alpha}{\sin^2 \theta_w} \left(\frac{m_H}{m_W} \right)^2 \delta(\hat{s} - m_H^2) .\end{aligned}\quad (5.66)$$

We find

$$\begin{aligned}\sigma \sim & \int_0^1 \frac{dx}{x} \left[\frac{\alpha}{2\pi \sin^2 \theta_w} \frac{(1-x)}{x} \right] \int_0^1 \frac{d\bar{x}}{\bar{x}} \left[\frac{\alpha}{2\pi \sin^2 \theta_w} \frac{(1-\bar{x})}{\bar{x}} \right] \\ & \cdot \sigma(W_L^+ W_L^- \rightarrow H^0) .\end{aligned}\quad (5.67)$$

The cross section for Higgs production by W fusion at high energy is indeed well approximated by the convolution of two distributions (5.63) with the cross section for $W_L^+ W_L^- \rightarrow H^0$.

The total cross section predicted by the peaking approximation (5.67) can be written more explicitly as^[51,59]

$$\begin{aligned}\sigma(e^+ e^- \rightarrow \nu^+ \nu^- \nu H^0) &= \frac{3\alpha}{32\pi \sin^6 \theta_w} \cdot \frac{s}{m_W^2} \\ & \cdot \left\{ \frac{1}{2} \left(1 + \frac{m_W^2}{s} \right) \log \frac{s}{m_W^2} - \left(1 - \frac{m_H^2}{s} \right) \right\} R .\end{aligned}\quad (5.68)$$

The magnitude of this total cross section is shown in Fig. 46. I should note that there are two approximations being made in this formula. The first is the

simplification of the kinematics made in eq. (5.64). This approximation is actually only qualitatively valid for center-of-mass energies below 1 TeV. The solid curves in Fig. 46 represent an exact calculation^[60] which integrates explicitly over the two W propagators. Based either on the approximation or on the exact result, we see that the cross section for Higgs boson production at a 1 TeV collider is very large up to Higgs masses of 400–500 GeV. The figure also indicates that the cross section is strongly energy-dependent.

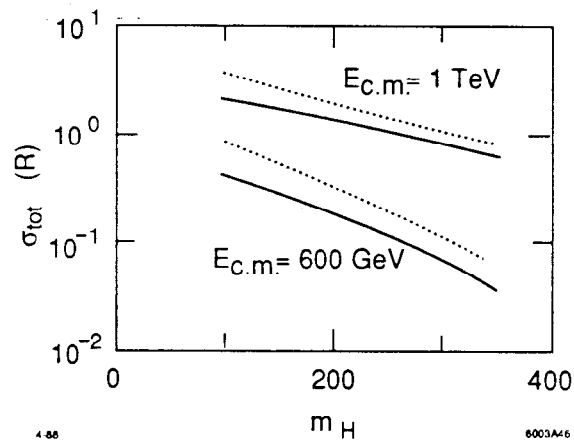


Figure 46. Total cross section for production of a standard neutral Higgs boson by W fusion. The solid curves represent an exact calculation assuming that the final Higgs is a narrow resonance. The dotted curves give the result of the peaking approximation, eq. (5.67).

The second approximation made in this analysis is that of taking the Higgs boson to be a narrow resonance. From Fig. 33, it is clear that this is a good approximation for Higgs boson masses below 600 GeV but becomes a very questionable procedure for Higgs boson masses of 1 TeV and above. At 1 TeV, the width of the standard neutral Higgs is 400 GeV, and so the Higgs boson subsides into a broad resonance on the continuum production of W^+W^- pairs. To calculate cross sections in this region, one should properly sum coherently all contributions to $e^+e^- \rightarrow \nu\bar{\nu}W^+W^-$. Such a calculation has been done by Gunion and Tofighi-Niaki,^[61] and the results are shown in Fig. 47.

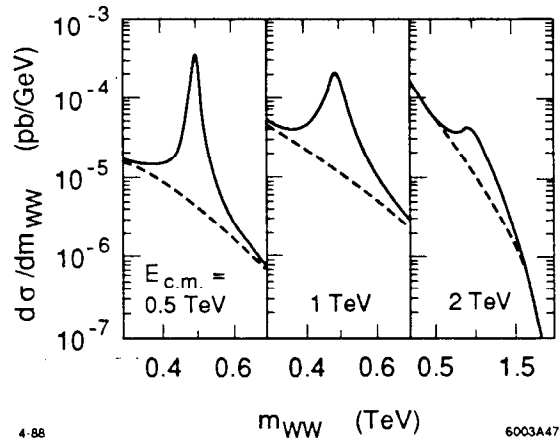


Figure 47. Calculations of the cross section for $e^+e^- \rightarrow \nu\bar{\nu}W^+W^-$, showing the Higgs boson as a W^+W^- resonance, from Ref. 61. The solid curves include a Higgs boson at the obvious mass; the dashed curves represent the result of a computation with $m_H = \infty$.

From the results of Fig. 47, it is clear that the WW process has the potential to probe the new interactions of W bosons associated with a high-mass, strongly interacting Higgs sector. To conclude this section, I would like to note that e^+e^- colliders offer one other window into strongly interacting Higgs dynamics. I have remarked already in Section 3.2 that technicolor theories predict new vector resonances in the region of 1 TeV. The model discussed there was of a maximal type, with a large spectrum of technipions. Other, minimal formulations of technicolor have no technipions, but they still must have the vector bosons of the new strong-interaction sector. In this case, the vector bosons couple mainly to the Goldstone scalars built from the technicolor particles, that is, by the Equivalence Theorem, to longitudinal W bosons. The effects can be quite dramatic. The technicolor rho resonance can appear as a final-state interaction resonance in any reaction that produces W pairs in a $J = 1$ state, for example, $e^+e^- \rightarrow W^+W^-$. Figure 48 shows the differential cross section for W pair-production in the minimal technicolor model as a function of energy, going through the position of the rho resonance.^[6] Unfortunately, as Figs. 47 and 48 make clear, the detailed study of new

strong interactions in the Higgs sector may require e^+e^- center-of-mass energies well above 1 TeV.

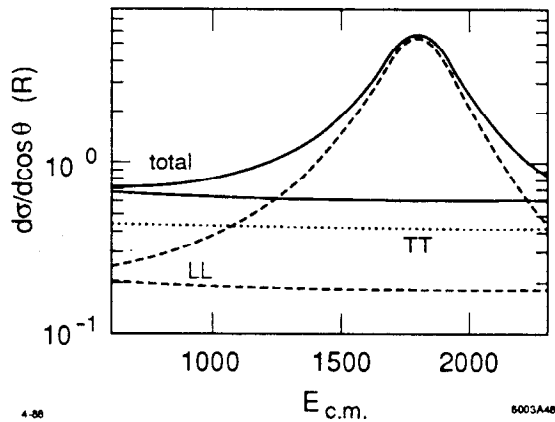


Figure 48. Effect of the rho resonance of technicolor strong interactions on the differential cross section for $e^+e^- \rightarrow W^+W^-$ at $\cos\theta = -0.5$. The dotted and dashed curves show, respectively, the contributions of the cross sections to transverse and longitudinal W pairs.

6. Conclusion

In these lectures, I have reviewed many aspects of the physics accessible to a high-energy e^+e^- collider. We began by considering the simplest processes which appear at such a machine, the pair-production of new particles. Electron-positron reactions already offer advantages at this simple level of experimentation, in providing a clean environment within which to detect new states and in allowing one to use polarization effects as a probe of the couplings of the particles which emerge. We then discussed searches for new composite and resonant structures. The fact that the basic standard model processes of e^+e^- colliders, such as Bhabha scattering, are weak and electromagnetic and thus understood in complete detail has been used to search for novel forms of coupling, and this will continue to be a powerful

technique at higher-energy machines. This fact also implies that a new gauge boson will stand out as an enormous effect, allowing detailed characterization of the additional force of Nature that such a boson would imply. Finally, we discussed the physics of the Higgs boson sector and vector boson mass generation. We saw that the interactions of Higgs bosons are mirrored in the behavior of W bosons at high energy, so that the detailed study of W boson physics gives a direct view into the Higgs dynamics. Taken all together, this experimental program offers the prospect of collecting the information we need to resolve the pressing question with which I began these lectures, the question of the mechanism of the spontaneous breaking of $SU(2) \times U(1)$ and the physics of the TeV scale. I look forward to the insights that these machines will provide.

Acknowledgements:

I thank Gary Feldman and the other members of the SLAC study group on the physics of a TeV linear collider for many discussions on the topic of these lectures.

REFERENCES

1. L. B. Okun, in *Proceedings of the 1981 International Symposium on Lepton and Photon Interactions at High Energies*, W. Pfeil, ed. (Univ. Bonn, 1981).
2. M. Veltman, *Nucl. Phys.* **B123**, 89 (1977).
3. P. Sikivie, L. Susskind, M. Voloshin, and V. Zakharov, *Nucl. Phys.* **B173**, 189 (1980).
4. F. Bulos, *et. al.*, in *Proceedings of the 1982 DPF Summer Study on Elementary Particles and Future Facilities*, (Snowmass, Colo.), R. Donaldson, R. Gustafson, and F. Paige, eds. (Fermilab, 1982).
5. J. Ellis, in *Proceedings of the XIV International Symposium on Multiparticle Dynamics*, P. Yager and J. F. Gunion, eds. (World Scientific, Singapore, 1984).
6. M. E. Peskin, in *Physics in Collision 4*, A. Seiden, ed. (Éditions Frontières, Gif-sur-Yvette, 1984).
7. G. Altarelli in *Proceedings of the Workshop on Physics at Future Accelerators (La Thuile)*, J. H. Mulvey, ed. (CERN, Geneva, 1987).
8. J. Ellis and F. Pauss, *ibid.*
9. C. Quigg, in these proceedings.
10. E. Eichten, I. Hinchliffe, K. D. Lane, and C. Quigg, *Rev. Mod. Phys.* **56**, 579 (1984).
11. G. Feldman, in these proceedings.
12. I. Hinchliffe, in *Proceedings of the 1982 DPF Summer Study on Elementary Particles and Future Facilities*, (Snowmass, Colo.), R. Donaldson, R. Gustafson, and F. Paige, eds. (Fermilab, 1982).
13. O. P. Sushkov, V. V. Flambauer, and I. B. Khriplovich, *Sov. J. Nucl. Phys.* **20**, 537 (1975).

14. W. Alles, Ch. Boyer, and A. Buras, *Nucl. Phys.* **B119**, 125 (1977).
15. B. Pendleton and G. Ross, *Phys. Lett.* **98B**, 291 (1981).
16. C. Hill, *Phys. Rev.* **D24**, 691 (1981).
17. J. Bagger, S. Dimopoulos, and E. Massó, *Nucl. Phys.* **B253**, 397 (1985).
18. M. Chanowitz, M. A. Furman, and I. Hinchliffe, *Phys. Lett.* **78B**, 285 (1978),
Nucl. Phys. **B153**, 402 (1979).
19. J. C. Pati and A. Salam, *Phys. Lett.* **58B**, 333 (1975).
20. G. Senjanović, F. Wilczek, and A. Zee, *Phys. Lett.* **141B**, 389 (1984).
21. H. P. Nilles, *Phys. Repts.* **110**, 1 (1984).
22. H. E. Haber and G. L. Kane, *Phys. Repts.* **117**, 75 (1985).
23. S. Raby in *From the Planck Scale to the Weak Scale*, H. Haber, ed. (World Scientific, Singapore, 1987).
24. R. M. Barnett, in *Proceedings of the Thirteenth SLAC Summer Institute on Particle Physics* (July, 1985), E. C. Brennan, ed. SLAC Report No. 296. (1986).
25. K. D. Lane and M. E. Peskin, in *Electroweak Interactions and Unified Theories*, J. Tran Thanh Van, ed. (Éditions Frontières, Derux, 1980).
26. E. Farhi and L. Susskind, *Phys. Repts.* **74**, 277 (1981).
27. K. Lane, in *Proceedings of the 1982 DPF Summer Study on Elementary Particles and Future Facilities*, (Snowmass, Colo.), R. Donaldson, R. Gustafson, and F. Paige, eds. (Fermilab, 1982).
28. C. R. Preitschopf, private communication.
29. T. Barklow and H. Haber, in preparation.
30. E. Farhi and L. Susskind, *Phys. Rev.* **D20**, 3404 (1979).
31. E. Eichten, K. D. Lane, and M. E. Peskin, *Phys. Rev. Lett.* **50**, 811 (1983).

32. S. Komamiya, in *Proceedings of the 1985 International Symposium on Lepton and Photon Interactions at High Energies*, M. Konuma and K. Takahashi, eds. (Nissha, Kyoto, 1986).
33. B. Schrempp, F. Schrempp, N. Wermes, and D. Zeppenfeld, *Nucl. Phys.* **B296**, 1 (1988).
34. M. Dine, V. Kaplunovsky, M. Mangano, C. Nappi, and N. Seiberg, *Nucl. Phys.* **B259**, 549 (1985).
35. G. Beall, M. Bander, and A. Soni, *Phys. Rev. Lett.* **48**, 848 (1982).
36. R. Ansari, *et. al.*, *Phys. Lett.* **195B**, 613 (1987).
37. L. S.-Durkin and P. Langacker *Phys. Lett.* **166B**, 436 (1986).
38. P. J. Franzini and F. J. Gilman, *Phys. Rev.* **D35**, 855 (1987).
39. I thank Haim Harari for discussions which aided this presentation.
40. P. Candelas, G. Horowitz, A. Strominger, and E. Witten, *Nucl Phys.* **B258**, 46 (1985).
41. M. E. Peskin, in *Proceedings of the Fourteenth SLAC Summer Institute on Particle Physics (July, 1986)*, E. C. Brennan, ed. SLAC Report No. 312. (1987).
42. F. Gürsey, P. Ramond, and P. Sikivie, *Phys. Lett.* **60B**, 177 (1976).
43. P. Langacker, R. W. Robinett, and J. L. Rosner, *Phys. Rev.* **D30**, 1470 (1984).
44. R. W. Robinett and J. L. Rosner, *Phys. Rev.* **D26**, 2396 (1982).
45. E. Witten, *Nucl. Phys.* **B258**, 75 (1985).
46. M. Cvetič, B. W. Lynn, and R. Stuart, in preparation.
47. C. Dib and F. J. Gilman, *Phys. Rev.* **D36**, 1337 (1987).
48. J. M. Cornwall, D. N. Levin, and G. Tiktopoulos, *Phys. Rev.* **D10**, 1145 (1974).

49. C. E. Vayonakis, *Lett. Nuov. Cim.* **17**, 383 (1976).
50. B. W. Lee, C. Quigg, and H. Thacker, *Phys. Rev.* **D16**, 1519 (1977).
51. M. Chanowitz and M. K. Gaillard, *Nucl. Phys.* **B261**, 379 (1985).
52. Z. Kunszt and D. E. Soper, *Nucl. Phys.* **B296**, 253 (1988).
53. J. Schwinger, *Phys. Rev.* **128**, 2425 (1962).
54. K. Hagiwara, R. D. Peccei, D. Zeppenfeld, and K. Hikasa, *Nucl. Phys.* **B282**, 253 (1987).
55. C. Ahn, B. Lynn, M. E. Peskin, and S. Selipsky, SLAC-PUB-4600 (1988).
56. G. L. Kane, W. W. Repko, and W. B. Rolnick, *Phys. Lett.* **148B**, 367 (1984).
57. S. Dawson, *Nucl. Phys.* **B249**, 42 (1985).
58. D. R. T. Jones and S. T. Petcov, *Phys. Lett.* **84B**, 440 (1979).
59. R. N. Cahn and S. Dawson, *Phys. Lett.* **136B**, 196 (1984).
60. R. N. Cahn, *Nucl. Phys.* **B255**, 341 (1985).
61. J. F. Gunion and A. Tofighi-Niaki, *Phys. Rev.* **D36**, 2671 (1987).